PIWIL2 downregulation in colon cancer promotes transposon activity and pro-tumorigenic phenotypes

Authors:

Alyssa Risner[1], Joyce Nair-Menon[1], Abhinav Cheedipudi[2], Joe R Delaney[3], Vamsi Gangaraju[3], Antonis Kourtidis[1]

Affiliations

[1]Department of Regenerative Medicine and Cell Biology, Medical University South Carolina, Charleston, SC

[2]University of South Carolina, Columbia, SC.

[3]Department of Biochemistry and Molecular Biology, Medical University South Carolina, Charleston, SC

Corresponding author: Antonis Kourtidis, kourtidi@musc.edu

ABSTRACT

Reactivation of transposable elements (TEs) in somatic tissues, particularly of LINE-1, is associated with disease by causing gene mutations and DNA damage. Previous work has shown that the PIWI pathway is crucial for TE suppression in the germline. However, the status and function of this pathway has not been well characterized in differentiated somatic cells and there is lack of consensus on the role of the pathway in somatic tumorigenesis. To shed light on this conundrum, we examined the PIWI pathway in colon cancer through a combination of bioinformatic analyses and cell-based assays. Shifted Weighted Annotation Network (SWAN) analysis revealed that the pathway experiences significant allelic losses in colon cancer and that PIWIL2, the main catalytic component of the pathway responsible for TE silencing, experiences the highest percent deletions. PIWIL2 is downregulated in colon tumors of advanced stage, nodal metastasis, and in certain subtypes, correlating with poor survival, while it is even downregulated in ulcerative colitis, an inflammatory bowel disease that predisposes to colon cancer. Knockout studies in colon epithelial Caco2 cells show that PIWIL2 depletion leads to increased anchorage-independent growth, increased LINE-1 levels and activity, and in DNA damage, altogether highlighting a tumor-suppressing role of PIWIL2 in the colon.

32 **SUMMARY STATEMENT**

33 This study investigates the PIWI-piRNA pathway in colon cancer using a nuanced bioinformatic and
34 cell-based approach, linking the downregulation of PIWIL2 to disease progression, transposable
35 element activation and DNA damage.

INTRODUCTION

Transposons, or transposable elements (TEs), are mobile DNA elements that make up approximately 45% of the human genome. Although they have been primarily studied in the germline and are overall considered inactive in differentiated somatic epithelial tissues, their reactivation has been shown to lead to a variety of diseases through the introduction of regulatory or protein coding changes when integrated into a new site (Beck et al., 2011, Elbarbary et al., 2016, Hancks and Kazazian, 2016). Additionally, recent studies have demonstrated that genomic instability, oncogene expression, and high mutation rates in approximately 50% of tumors are linked to increased TE activity (Tubio et al., 2014, Jang et al., 2019).

Among the several TE families existing in the human genome, the Long Interspersed Nuclear Element-1 (LINE-1) is the most abundant and the only autonomously mobilizing TE family in humans(Beck et al., 2011). While most copies of the LINE-1 TE are inactive due to truncations and mutations, 100-150 copies are functionally active in disease(Wang et al., 2024, Beck et al., 2010, Tubio et al., 2014, Rodriguez-Martin et al., 2020). The functional LINE-1 copies contain protein-coding open reading frames (ORFs), ORF1 and ORF2, that encode an RNA-binding protein and reverse transcriptase, respectively, to facilitate reverse transcription of the LINE1 RNA transcript(Beck et al., 2011, Elbarbary et al., 2016, Hancks and Kazazian, 2016). Reactivation of LINE-1 has been frequently observed in somatic tissues and particularly in the gastrointestinal tract, where it has been associated with colon cancer, the second most frequent and third deadliest cancer type in both sexes(Pitkanen et al., 2014, Solyom et al., 2012, Ewing et al., 2015, Tubio et al., 2014, Zhuo et al., 2015, Nam et al., 2023, Siegel et al., 2024). Indeed, recurrent LINE-1 insertions have been identified to cause mutations in known oncogenes or tumor suppressors such as APC, a key initiating event in colorectal tumorigenesis, indicating that LINE-1 retro-transposition events have the ability to serve as tumor-initiating events in colon cancer(Cajuso et al., 2019, Scott et al., 2016, Miki et al., 1992). In fact, colon tumors are significantly enriched with somatic retro-transpositions(Rodriguez-Martin et al., 2020). However, the reasons for increased TE activity in these tumors are still poorly understood.

Mechanisms of TE regulation previously described in the germline include DNA methylation and histone modifications of LINE-1 loci, as well as RNA interference by small RNAs through the PIWI pathway(Kuramochi-Miyagawa et al., 2008, Sigurdsson et al., 2012, Ariumi, 2016, Berrens et al., 2017, Walter et al., 2016). The PIWI pathway was first described in *Drosophila* to suppress TEs in the germline and to be required for spermatogenesis(Ku and Lin, 2014). PIWI proteins are members of the Argonaute family of endoribonucleases that bind PIWI interacting RNAs (piRNAs), a distinct class of small non-coding RNAs that are 24-32 nucleotides in length, altogether forming the piRNA-induced silencing complex (piRISC)(Siomi et al., 2011). Most piRNAs are derived from piRNA clusters within the genome,

which are also locations of a large number of truncated TEs (Siomi et al., 2011). piRISC recognizes piRNA - complementary RNA transcripts of TEs in their cytosolic phase and cleaves them, subsequently preventing retro-transposition and DNA mutagenesis(Ramat and Simonelig, 2021, Watanabe and Lin, 2014, Weick and Miska, 2014).

The PIWI-piRNA mechanism is conserved throughout evolution, including in mammals, where it has been found to be required for germline maintenance in mice(Unhavaithaya et al., 2009, Sun et al., 2022, Kuramochi-Miyagawa et al., 2008, Li et al., 2021). In humans, there are four PIWI protein members, namely PIWIL1, PIWIL2, PIWIL3 and PIWIL4(Zeng et al., 2020). In addition to PIWI proteins, the TE targeting function of piRISC is enabled by a number of additional protein components, including the Tudor family of proteins that act as protein scaffolds, as well as by RNA helicases, such as MOV10L1 and DDX4(Siomi et al., 2010, Mathioudakis et al., 2012, Reuter et al., 2009, Gao et al., 2024, Frost et al., 2010, Vourekas et al., 2015, Fu et al., 2019, Li et al., 2021, Wenda et al., 2017). Although it was previously thought that PIWI proteins were germline - specific in humans, a recent study that sought to characterize their expression patterns across multiple tissue types showed that PIWI proteins, namely PIWIL2 and PIWIL4, are also expressed substantially in somatic tissues(Meseure et al., 2020).

In addition to their expression in normal somatic tissues, a number of studies have suggested that PIWI proteins are overexpressed in somatic tumors and act as oncogenes, in a similar fashion to the overall scheme of re-expression of stem cell and germline markers in tumors; however, other studies have shown that PIWI proteins in fact act as tumor suppressors, altogether exposing a lack of consensus on the function of PIWI proteins in somatic tissues and tumors (Lee et al., 2006, Lu et al., 2012, Wang et al., 2015, Zeng et al., 2017, Eckstein et al., 2018, Meseure et al., 2020, Kishani Farahani et al., 2023, Shi et al., 2020). This is particularly the case for PIWIL2, which is the key endoribonuclease that binds primary piRNAs in piRISC to target TE RNA transcripts for degradation, including LINE-1(Siomi and Siomi, 2015, De Fazio et al., 2011). Still, the function of PIWIL2 in differentiated epithelial tissues and its role in tumorigenesis has not been well characterized(Yan et al., 2011, Ross et al., 2014b, Peng and Lin, 2013, Martinez et al., 2015, Jacobs et al., 2016, Gao, 2008, He et al., 2010, Liu et al., 2010). Previous *in vitro* work studying PIWIL2 has been primarily conducted in transformed cancer cell lines, or in commonly used cell lines such as HEK-293 cells, none of which are representative of the normal differentiated epithelium. Here, we aimed to elucidate the expression and function of the PIWI complex in colon cancer, through performing bioinformatic analyses and functional assays in colon epithelial cells.

RESULTS

SWAN analysis identifies dysregulation of the PIWI pathway in colon cancer

To decipher the expression and role of the PIWI-piRNA pathway in colon cancer, we first used bioinformatic tools to investigate the status of key proteins of the pathway through mining data from The Cancer Genome Atlas (TCGA). To do this, we used the Shifted Weighted Annotation Network (SWAN) algorithm, which has the capability to interrogate pathway and copy-number alterations (CNAs) within the TCGA data set(Bowers et al., 2022). Networks in the algorithm are scored based on the number of interactions within the pathway and if haploinsufficiency data are available for the dataset. The Single-pathway SWAN algorithm was used to perform Gene Ontology Biological Process Analysis on the PIWI-piRNA metabolic pathway in the TCGA colon adenocarcinoma (COAD) dataset (**Fig 1**). The pathway was scored by the SWAN algorithm as overall haploinsufficient **(Fig 1A**). Allelic losses or gains were then mapped to each respective chromosome by the algorithm (**Fig 1B**). This analysis showed that there is not a single “hot spot” across the genome where all the observed allelic losses or gains are concentrated, but that these are dispersed throughout the genome. Notably, PIWIL2, which is the main catalytic component of the primary piRNA pathway involved in TE regulation, experienced the highest percent deletion and allelic losses of the pathway queried (**Fig 1C**). PIWIL1 and PIWIL4 were not significantly enriched in the SWAN algorithm with gains or losses, and PIWIL3 was excluded from the pathway by the algorithm. Proteins required for both primary and secondary piRNA processing experienced allelic losses, including the nuclease EXD1; RNA helicase DDX4 (Vasa in *Drosophila*; MVH in mice); PLD6 (Zucchini in *Drosophila*; mitoPLD in mice) that generates the 5’ end of primary piRNAs; RNA helicase MOV10L1 that is required for stabilizing the primary piRNA transcript; as well as TDRD1 and TDRD9 that are required for stabilization of the complex and piRNA loading(Yang et al., 2016, Wenda et al., 2017, Nishimasu et al., 2012, Han et al., 2015, Vourekas et al., 2015, Zhang et al., 2019, Mathioudakis et al., 2012). Interestingly, four components of the pathway experienced high percentages of allelic amplifications and allelic gains in the COAD dataset, including TDRD12, TDRKH, ASZ1 and FKBP6. TDRD12 is a binding partner of EXD1 while TDRKH is required for 3’end processing of piRNAs(Pandey et al., 2013, Saxe et al., 2013). ASZ1 is required for phased piRNA biogenesis through the stabilization of PIWIL2 and PIWIL4, while FKBP6 is a co-chaperone to facilitate piRNA loading (Ma et al., 2009, Ikeda et al., 2022, Saxe et al., 2013, Xiol et al., 2012). Furthermore, we queried whether PIWIL2 allelic loss correlates with patient survival using the cBioportal copy number alteration (CNA) tool; indeed allelic loss of PIWIL2 correlates with poorer patient survival compared to patients without an allelic loss (**Fig 1D**). The results from the SWAN and cBioportal analyses highlight the overall loss of regulation of the entire piRNA biogenesis pathway in colon cancer and identify PIWIL2 as a top candidate for the loss of pathway’s regulation.

PIWIL2 is downregulated in colon cancer in correlation with disease progression

Next, we queried PIWIL2 expression levels in the TCGA dataset using the University of Alabama at Birmingham CANcer data analysis portal (UALCAN) (**Fig 2, Fig 3**). A general overview of PIWIL2 expression among all tissues and cancers included in the database confirms the high expression of PIWIL2 in normal tissues particularly of gastrointestinal origin, namely colon, rectal, and gastric (**Fig 2**). We then interrogated the COAD (colon adenocarcinoma) dataset to examine PIWIL2 mRNA expression stratified by normal vs: primary tumor; tumor stages; nodal metastasis; p53 status; histological subtype (adenocarcinoma, mucinous adenocarcinoma); microsatellite stability; age; weight; race; and biological sex (**Fig 3A-J**). Comparisons between normal and primary tumors showed decreased PIWIL2 levels in tumors, as well as when tumors were stratified by stage I-IV (**Fig 3A,B**). Due to high variance in expression, this downregulation of PIWIL2 only reached statistical significance in the transition to stage IV (**Fig 3B**); however, downregulation of PIWIL2 in tumors was significant when the tumors were stratified by lymph node metastasis, particularly in N0 tumors compared to normal and between N0 and N2 tumors, denoting correlation of PIWIL2 both with early transformation at N0 and with tumor aggressiveness at N2 (**Fig 3C**). Interestingly, PIWIL2 downregulation does not correlate with p53 status (**Fig 3D**); however, PIWIL2 was significantly downregulated in adenocarcinomas compared to normal tissues, and even more downregulated in mucinous adenocarcinomas (**Fig 3E**). Mucinous adenocarcinomas possess a high degree of microsatellite instability, which is a feature that is used to categorize colon tumors in MSI-H (microsatellite instability - high), MSI-L (microsatellite instability - low), and MSS (microsatellite stable). Since the UALCAN database does not include the option of stratifying tumors based on microsatellite instability, we used GEPIA2(Tang et al., 2019) to examine expression of PIWIL2 in these sub-categories of tumors. Interestingly, PIWIL2 is downregulated in MSI-L tumors and even more significantly in MSI-H tumors, compared to MSS tumors (**Fig. 3F**). This result is in agreement with the downregulation of PIWIL2 in the mucinous adenocarcinomas, which are microsatellite unstable. PIWIL2 also seems to be progressively downregulated by age, where MSI-H tumors are also more prevalent (Guidoboni et al., 2001) (**Fig 3G**). Finally, there were no statistically significant differences in PIWIL2 expression by weight, race, or biological sex (**Fig 3H,I,J**). Low PIWIL2 expression in colon tumors was also correlated with poor patient survival among all tumor stages, when stratified by stages 1-3 combined, and even more pronounced in stage 4, using the Kaplan-Meier Plotter web-based tool (**Fig 3K-M**), which is in agreement with the CNA data (**Fig 1D**).

Furthermore, examination of the methylation levels of the PIWIL2 promoter using UALCAN showed that this was significantly elevated in colon tumors overall, indicated by a higher methylation beta-value, as well as when these tumors were stratified by stage, nodal metastasis; p53 status; histological subtype; age: biological sex; weight; and race (**Fig 4**). These findings indicate that PIWIL2 expression is suppressed across colon cancer due, in part, to promoter methylation and microsatellite instability.

173

174 **PIWIL2 is also downregulated in ulcerative colitis**

175 Since we identified downregulation of PIWIL2 in colon tumors beginning from early forms of the disease,
176 such as in N0 tumors, we then sought to examine the status of PIWIL2 in precancerous conditions in
177 the colon, such as in inflammatory bowel disease that significantly increases the risk for colon
178 cancer(Kim and Chang, 2014, Gordon et al., 2018). To do this, we examined the expression levels of
179 members of the PIWI pathway that we identified using the SWAN analysis, using expression data from
180 patients with ulcerative colitis, one of the main manifestations of inflammatory bowel disease, available
181 through the PreMedIBD database(Linggi et al., 2021). This analysis showed that out of all the members
182 of the PIWI-piRNA pathway that were queried, PIWIL2 was the gene that was more predominantly
183 downregulated in ulcerative colitis (**Fig 5**). This further denotes PIWIL2 as the member of the pathway
184 that is potentially most critical for tumor initiation. Altogether, the above analyses demonstrate that the
185 PIWI pathway is dysregulated in colon cancer, particularly its main component PIWIL2, and its
186 downregulation correlates with disease initiation and progression.

187

188 **PIWIL2 depletion in colon epithelial cells promotes pro-tumorigenic behavior**

189 Given that PIWIL2 exhibits the most allelic losses in the entire PIWI pathway and is also downregulated
190 in ulcerative colitis and colon cancer correlating with disease progression (**Fig 1C, Fig 3, Fig 4, Fig 5**),
191 we sought to investigate whether loss of PIWIL2 may indeed promote pro-tumorigenic phenotypes. To
192 do this, we used Caco2 colon epithelial cells, a broadly used in vitro model of the well-differentiated
193 colonic epithelium(Grasset et al., 1984, Hidalgo et al., 1989, Sambuy et al., 2005). We first confirmed
194 that PIWI proteins were expressed in these cells, by examining our publicly available RNA-sequencing
195 data(Daulagala et al., 2024). The data confirmed expression of PIWIL2 and PIWIL4 in Caco2 cells, but
196 not of PIWIL1 and PIWIL3 (**Supplemental Table 1**). We then generated a PIWIL2 CRISPR/Cas9
197 mediated knockout (KO) in Caco2 cells. The PIWIL2 KO was overall not well tolerated by these cells,
198 since most cells didn't survive selection; however, we isolated cells where we confirmed 50%
199 downregulation of PIWIL2 by qRT-PCR (**Fig 6A**) and by western blot, when assessing the full length
200 PIWIL2 at the predicted molecular weight of 109 kDa and when quantified over 3 biological replicates
201 (**Fig 6B, C**).

202

203 We then sought to assess the potential phenotypic effects of PIWIL2 depletion in these cells on cell
204 proliferation, since increased proliferation is an indication of pro-tumorigenic behavior. To do this, we
205 used the xCELLigence Real-Time Cell Analysis (RTCA) system, to monitor cell proliferation rates in
206 standard 2-dimensional conditions and in real time (**Fig 6D**). Interestingly, the PIWIL2 KO cells had a
207 significantly lower proliferation rate indicated by a slower growth curve, than the Caco2 WT control

cells, taking approximately twice as long for the KO cells to reach confluency at 48 hours compared to WT cells, which reached confluency in 26 hours. This shows that PIWIL2 depletion has negative effects on cell proliferation in standard 2-dimensional cultures.

We then examined the ability of the PIWIL2 KO cells to grow in anchorage-independent conditions, which is a hallmark of pro-tumorigenic transformation. To do this, we cultured cells using a low attachment plate assay to determine if the PIWIL2 KO cells could form spheroids in these conditions (**Fig 6E-I**). Caco2 WT cells were able to form only small and very few spheroids after 10 days, which is expected since these cells are well-differentiated epithelial cells and not expected to grow in anchorage-independent conditions(Kourtidis et al., 2015). However, the PIWIL2 KO cells grew into much larger spheroids that exhibited a significantly larger area, perimeter and diameter, and were relatively symmetrical, when considering there were no significant changes in circularity. These data demonstrate that PIWIL2 KO in Caco2 cells, although results in a lower proliferation rate in 2-dimensional cultures, it promotes cell growth in an anchorage independent manner, indicating a pro-tumorigenic potential of these cells.

PIWIL2 depletion increases the levels and activity of the LINE-1 transposable element

Since PIWIL2 is the main enzymatic component of the PIWI pathway responsible for TE targeting and suppression, we investigated whether PIWIL2 depletion would promote TE upregulation and activation. We first examined whether LINE-1 levels were increased in the PIWIL2 KO cells by qRT-PCR of the L1RE1 RNA transcript, which includes the first ORF of the LINE-1 mRNA that encodes the ORF1p RNA binding protein required for LINE-1 retro-transposition(Beck et al., 2011, Elbarbary et al., 2016). PIWIL2 depletion increased the L1RE1 transcript by 1.5-fold (**Fig 7A**), showing that LINE-1 levels are indeed upregulated. To examine whether the increased LINE-1 levels upon PIWIL2 depletion were also accompanied by increased retro-transposition activity, we utilized a retro-transposition LINE1-GFP reporter assay(Moran et al., 1996, Ostertag et al., 2000, Garcia-Perez et al., 2010, Kopera et al., 2016). In this assay, a plasmid with a full-length retro-transposition competent LINE-1 element produces GFP only when retro-transposition occurs and is an indicator of TE activity within the cell (denoted LINE1-GFP). Additionally, the assay uses a negative control plasmid with an inactive LINE-1 element that contains a defective ORF1p protein (LINE1 inactive (-)) that is unable to retro-transpose and produce GFP. Caco2 WT or PIWIL2 KO cells were transfected with either a constitutively active GFP reporter plasmid (pCEP4+) to determine transfection efficiency, the LINE1-GFP retro-transposition reporter, or the LINE1 inactive (-) plasmid as a negative control. After 48 hours, transfected Caco2 WT and PIWIL2 KO cells were placed in puromycin selection for 4 days and then imaged by fluorescence microscopy to identify GFP positive cells (**Fig 7B**). The average percent of positive GFP expressing cells was

243 normalized to the transfection efficiency of each cell line for comparison (**Fig 7C**). Caco2 WT + LINE1-
244 GFP fluorescence was minimal and not significantly different compared to Caco2 WT LINE-1 inactive
245 (-) cells, indicating there is minimal LINE-1 activity in the Caco2 WT cells. However, PIWIL2 KO +
246 LINE1-GFP exhibited significantly higher LINE-1 activity compared to the PIWIL2 KO + LINE1 inactive
247 (-) cells, indicating specific LINE-1 activation in the PIWIL2 KO cells; this increased activity was also
248 significantly higher compared to Caco2 WT + LINE1-GFP cells, demonstrating that PIWL2 depletion
249 not only increases LINE-1 mRNA transcript levels, but also LINE1 activity in colon epithelial Caco2
250 cells.
251
252 **PIWIL2 depletion promotes DNA damage**
253 The DNA insertional activity of TEs and especially of LINE-1 elements can cause DNA damage, which
254 is a hallmark of cancer (Gasior et al., 2006, Hanahan and Weinberg, 2011). Therefore, we examined
255 whether the increased LINE-1 activity upon PIWIL2 depletion in Caco2 cells (**Fig 7B,C**) also results in
256 DNA damage in these cells (**Fig 8**). Immunofluorescent staining followed by confocal microscopy of
257 Caco2 WT and PIWIL2 KO cells for γH2AX, a phosphorylated histone marker of DNA double stranded
258 breaks(Kuo and Yang, 2008), revealed that there was a significant increase in the number of γH2AX
259 foci per cell (**Fig 8A,B**). We also confirmed increased levels of γH2AX compared to total H2AX by
260 immunoblotting (**Fig 8C**). These results demonstrate that PIWIL2 depletion in the somatic, well-
261 differentiated colon epithelial Caco2 cells results in up regulation of transposon levels and activity, as
262 well as in subsequent increased DNA damage, which are all promoters of pro-tumorigenic
263 transformation. These findings, taken together with the dysregulation or the PIWI pathway and
264 downregulation of PIWIL2 in colon tumors, as well as with the significantly increased ability of the
265 PIWIL2 KO cells to grow in anchorage-independent conditions, underscore a tumor-suppressing role
266 of PIWIL2 in the colon.
267
268 **DISCUSSION**
269 Prior studies have shown that the activation of TEs in tumors, including colon cancer, was frequent,
270 although little is known regarding the potential mechanisms of TE activation (Pitkanen et al., 2014,
271 Ewing et al., 2015, Solyom et al., 2012). Recently, the PIWI pathway, which is well-established to
272 suppress transposons in the germline, has also been shown to be expressed in the soma and be
273 implicated in cancer(Ross et al., 2014a, Siomi et al., 2011). However, reports regarding the presence
274 of PIWI proteins in somatic tissues and the role of this pathway in tumorigenesis have been conflicting,
275 with some supporting a tumor-suppressing and others a tumor-promoting role of the pathway. Our
276 bioinformatic analysis, as well as our RNAseq, qRT-PCR, and protein expression data, confirm
277 expression of PIWIL2, the key regulator of the pathway, in the colon and in the well-differentiated colon

278 epithelial Caco2 cells (**Fig. 2,3,6,Supplemental Table 1**). Our data also show that the pathway
279 experiences significant allelic losses and its expression is downregulated in colon adenocarcinoma,
280 with PIWIL2 having the highest percentage of deletions and allelic losses within the pathway (**Fig. 1**).
281 Both PIWIL2 allelic loses and downregulation also correlate with poor patient survival. Furthermore,
282 knockout of PIWIL2 in Caco2 cells resulted in increased expression and activity of the LINE-1 TE, the
283 most abundant and only autonomous TE in humans, as well as in DNA damage and in anchorage-
284 independent growth, all hallmarks of pro-tumorigenic transformation (**Fig 6,7,8**). Altogether, the data
285 support the idea that PIWIL2 acts as a tumor suppressor in the colon.

286 Furthermore, when we interrogated PIWIL2 expression levels in the TCGA dataset by UALCAN
287 analysis, PIWIL2 loss was more prevalent in the mucinous adenocarcinoma subtype of colon cancer
288 (**Fig 3E**), which is found in 10%-20% of colon cancer patients and is characterized by ≥50% of the
289 tumor volume consisting of extracellular mucins(Fleming et al., 2012, Luo et al., 2019, Huang et al.,
290 2021). Studies have also shown that mucinous adenocarcinoma tumors exhibit a higher frequency of
291 microsatellite instability, CpG island methylation, and lower frequency of p53 mutations(Luo et al., 2019,
292 Huang et al., 2021). Indeed, PIWIL2 downregulation in colon tumors seems to correlate with
293 microsatellite instability, independently of p53 status (**Fig. 3D,F**). These findings further suggest the
294 involvement TE mobility in tumorigenesis, since retrotransposons like LINE-1 are known to give rise to
295 de novo microsatellites during retro-transposition events due to internal proto-microsatellite sequences
296 and poly-A mononucleotide repeats (Grandi and An, 2013). Since PIWIL2 downregulation seems to be
297 independent of p53 status, which is key for maintaining genome integrity, it is likely that PIWIL2
298 dysregulation in microsatellite tumors is a potential mechanism of LINE-1 activation which would be
299 interesting to be further interrogated.

300 Our database examination also showed that PIWL2 is downregulated in samples from patients with
301 ulcerative colitis, which highlights a gap in current research since the PIWI pathway has not been
302 previously studied in colitis and in inflammatory bowel disease (**Fig 5**). A few studies have indicated
303 that there is upregulation of LINE-1 elements in inflammatory bowel disease, particularly in Crohn's
304 Disease; however, the information on transposon expression and their regulation in these diseases is
305 still very limited(Kanke et al., 2022, Wang et al., 2017). Given the above and that colitis and
306 inflammatory bowel disease overall strongly predispose for colon cancer, it would be interesting to
307 examine whether this PIWIL2 downregulation is a contributing factor to this predisposition, through
308 upregulation of LINE elements in these diseases.

309 Interestingly, our *in vitro* studies showed that only a partial knockout of PIWIL2 is tolerated by Caco2
310 cells, which correlates with the haploinsufficiency identified by the SWAN algorithm (**Fig 1,6A-C**). In
311 fact, this low tolerance for PIWIL2 loss may be due to the ensuing DNA damage caused by PIWIL2

312 downregulation (**Fig. 8**) and may also explain their lower proliferation rates in regular 2-dimensional
313 cultures (**Fig. 6D**). However, we found that even a 50% depletion of PIWIL2 was able to significantly
314 promote anchorage independent growth of Caco2 cells, which are otherwise well-differentiated, and
315 don't grow efficiently under these conditions (**Fig. 6E**). Acquisition of anchorage independent growth
316 capability is a key event in epithelial cell pro-tumorigenic transformation. Furthermore, the increased
317 DNA damage upon depletion of PIWIL2 was accompanied by increased levels and activity of the LINE-
318 1 TE, indicating that TE regulation and silencing is disrupted upon PIWIL2 depletion (**Fig 7**). Both TE
319 activation and DNA damage are driver events in tumorigenesis (Cajuso et al., 2019, Scott et al., 2016,
320 Miki et al., 1992, Gasior et al., 2006); therefore, these findings, taken together with our current data
321 showing early downregulation of PIWIL2 in colon tumors or even in pre-cancerous diseases,
322 underscore a potential role of PIWIL2 in early colon tumorigenesis, which deems further investigation.

323 Together, the data support a tumor suppressing role for PIWIL2 in somatic cells and in colon
324 tumorigenesis. However, PIWIL2 is part of a larger protein complex (piRISC) and the SWAN analysis
325 identified additional members of the PIWI-piRNA pathway and of piRISC as also significantly
326 downregulated. For example, other top targets from the SWAN analysis include the exonuclease EXD1
327 found in pi-bodies, the RNA helicases DDX4 and MOV10L1, PLD6, and several members of the Tudor
328 family of proteins that are key for the functionality of piRISC. These proteins have also been identified
329 to be dysregulated in other cancer types, mainly breast and ovarian cancers, but they have not been
330 studied in the colonic epithelium, since this is still a novel and ongoing field of investigation(Olotu et al.,
331 2024, Kim et al., 2014, Lee et al., 2020). Therefore, it would be of particular interest to further investigate
332 these additional PIWI pathway components and their roles in suppressing TEs in colonic diseases. In
333 summary, our work, through using a nuanced bioinformatic approach and by performing cell - based
334 assays, sheds light into the currently conflicting views about the role of the PIWI pathway in somatic
335 tissues and in cancer, opening future directions of investigation that will fully assess the tumor
336 suppressing potential of this pathway.

337

338 **METHODS**

339 **Bioinformatic Analysis**

340 Multiple bioinformatic tools were used throughout this study to investigate changes in the PIWI protein
341 pathway using data from The Cancer Genome Atlas (TCGA). The analytical tools are detailed below.

342

343 Shifted Weighted Annotation Network (SWAN): SWAN is an analytical tool used to interrogate pathway
344 and copy-number alterations (CNAs) within the TCGA data set and can be found at the following
345 webpage: https://www.delaneyapps.com/. The Single-pathway SWAN tool was used to perform Gene

346 Ontology Biological Process Analysis on the piRNA metabolic pathway in COAD with a 0.001
347 significance threshold over 1000 permutations of the algorithm. RNA data was integrated with CNA
348 data for this analysis and a Wilcoxon rank test was calculated as described (Bowers et al., 2022).
349
350 cBioportal: cBioportal is another open-source web-based tool to visualize multidimensional cancer
351 genomics data sets, including data from TCGA Pan Cancer Atlas (Cerami et al., 2012, Gao et al., 2013,
352 de Bruijn et al., 2023). This tool can be found at the following webpage: https://www.cbioportal.org. The
353 TCGA COAD data set was selected and then queried for samples with shallow deletion CNAs (loss of
354 one allele; HETLOSS) of PIWIL2 and a plot of Overall Survival was generated using the
355 Comparison/Survival Tool.
356
357 UALCAN: UALCAN is a web-based tool from the University of Alabama at Birmingham that allows users
358 to stratify TCGA data for more in-depth analysis of TCGA expression profiles. This tool can be found at
359 the following webpage: https://ualcan.path.uab.edu/. A pan-cancer analysis of PIWIL2 expression was
360 performed across multiple tumor types to compare overall expression in normal and tumor samples.
361 PIWIL2 expression and methylation was then queried in the TCGA colon adenocarcinoma (COAD) data
362 set and stratified by normal vs tumor, tumor stage, nodal metastasis, p53 status, histological subtype,
363 biological sex, age, weight, and race. The median and interquartile range is displayed, and statistical
364 significance was calculated by the UALCAN algorithm using a Welch's T-test as previously described
365 (Chandrashekar et al., 2017, Chandrashekar et al., 2022). Results were exported from UALCAN, and
366 graphical displays were made in Prism 10 (Graphpad).
367
368 GEPIA2: GEPIA2 is an interactive web-based tool for analyzing RNA-seq data from the TCGA and
369 GTEx projects that can be found at the following webpage: http://gepia2.cancer-pku.cn/#index. The
370 single gene analysis search for PIWIL2 was used to plot box plots stratified by cancer subtype (MSS,
371 MSI-L, MSI-H) of gene expression. For this study, the median expression of colon adenocarcinoma
372 (COAD) was plotted from TCGA data available with the upper and lower quartiles. The GEPIA2
373 program calculated statistical significance using a one-way ANOVA. A $\log_2$-fold-change of 0.5 and p-
374 value of 0.5 were set as thresholds for the analysis(Tang et al., 2019).
375
376 Kaplan-Meier Plotter: This web-based tool is capable of correlating mRNA expression data and survival
377 data of colon cancer datasets from the Gene Expression Omibus (Gyorffy, 2024). A hazard ratio with
378 95% confidence intervals and logrank P value are calculated by the program. PIWIL2 was interrogated
379 to determine Regression Free Survival and stratified by all tumor stages, stages 1-3 combined and

380 stage 4 alone. This web-based tool can be found at the following webpage https://www.kmplot.com
381 (Gyorffy, 2024).
382
383 PreMedIBD: PreMedIBD is a web-based data mining tool for meta-analysis of ulcerative colitis tissue
384 gene expression. This tool can be found at the following webpage: https://premedibd.com/genes.html.
385 PIWIL2, PIWIL4, DDX4, PLD6, EXD1, TDRD1, TDRD9, TDRD12 and MOV10L1 were queried and the
386 log2-Fold gene expression changes between ulcerative colitis patients and non-IBD controls were
387 determined for each gene. The meta-analysis was calculated as previously described using a random
388 effects model and shows the meta-log2-Fold change and 95% confidence interval(Linggi et al., 2021).
389 A $\log_2$-fold-change of 0.5 was used as a threshold for significance. Datasets used are available in the
390 Gene Expression Omnibus: GSE13367, GSE9452, GSE53306, GSE38713, GSE47908, GSE73661,
391 GSE114527, GSE87466.
392
393 **Cell Culture**
394 Caco2 colon epithelial cells (ATCC, #HTB-37) were cultured in MEM (Corning, #10-010-CV) with 10%
395 fetal bovine serum (FBS) (Gibco,Fetal Bovine Serum Qualified One Shot #A31605-02), 1 mM sodium
396 pyruvate (Gibco, #11360-070), and 1x non-essential amino-acids (NEAA) solution (Gibco, #11140-050).
397 Cells were maintained at 37°C with 5% CO_2. The Caco2 PIWIL2 knockout (KO) cell line was generated
398 using CRISPR/Cas9 technology in collaboration with the Cell Models Core as part of the Medical
399 University of South Carolina COBRE in Digestive and Liver Disease following the protocol by Ran et
400 al.(Ran et al., 2013) The sgRNA sequence was designed to target exon 14 of PIWIL2
401 (sense:CACCGCCAATGAACTGATGCGTTGG/antisense: AAACCCAACGCATCAGTTCATTGGC)
402 using the online Synthego tool (www.synthego.com) and synthesized by Integrated DNA Technologies,
403 IDT. This PIWIL2-targeting sgRNA was cloned into the PX459 pSPCas9(BB)-2A-Puro vector and
404 Caco2 cells were transfected with 30 µg the sgRNA-containing vector using Lipofectamine 3000
405 (Invitrogen) according to the manufacturer's protocol. After 24 hours, cells were selected with 5 µg/ml
406 puromycin for 48 h. Successfully transfected cells were seeded to obtain single colonies, which were
407 picked and expanded for screening by western blot and qPCR. PCR using primers designed to amplify
408 the target region was performed (Forward1: CTCGAACACCTGGGCTCAAGCG and Reverse1:
409 ACCACGCACAGAGGTTCATACC and Forward2: ATCACATTCACCTTCCTAAGAGA and Reverse2:
410 GACCACGCACAGAGGTTCAT)
411
412 **RNA isolation, qPCR, and RNAseq of Caco2 cells**
413 RNA was isolated by adding 1ml of Trizol (Invitrogen # 15596018), incubating the sample at RT for 5
414 minutes then using the PureLink RNA mini kit (Invitrogen #12183018A) for total RNA. Final RNA

concentrations and purity were determined by using a NanoDrop spectrophotometer. RNA was converted to cDNA using the High Capacity cDNA Reverse Transcriptase Kit (Applied Biosystems #4368814). qPCR reactions were performed using the Taqman FAST Universal PCR master mix (Applied Biosystems #4352042), in a BioRad CFX96 Touch/Connect real time quantitative PCR machine. Data were analyzed and normalized to 18S ribosomal RNA by ΔΔCt calculations to calculate fold change compared to control samples. The Caco2 RNA sequencing that was used to extract the PIWI1-4 expression data shown in Supplemental Table 1 have been previously published and are publicly available in the GEO public database, under the accession number GSE156860(Daulagala et al., 2024).

Immunoblotting

Whole-cell protein lysates were obtained using RIPA buffer (50 mM Tris, pH 7.4, 150 mM NaCl, 1% NP-40, 0.5% deoxycholic acid, and 0.1% SDS) supplemented with protease inhibitor (RPI Research Products, #P50750-1) and phosphatase inhibitor (Thermo Fisher Scientific, Halt Phosphatase inhibitor cocktail, #1862495) at 1:100 dilution. Cell culture plates were scraped with a cell scraper, lysates were homogenized through a syringe, and then cleared by centrifugation at 15,000 rpm for 5 minutes. Protein quantification was performed using a Pierce BCA Protein Assay (Thermo Fisher Scientific, #23227). Protein extracts were mixed with Laemmli sample buffer and separated by SDS–PAGE using 4–20% Tris-Glycine eXtended (TGX) gels (Bio-Rad) and transferred to 0.2 µm nitrocellulose membranes (Bio-Rad) with the Trans-Blot Turbo Transfer System (Bio-Rad). Transfer efficiency was determined using a Ponceau S stain (Thermo Fisher Scientific, #A40000279). Membranes were blocked in 3% milk for 45 minutes and incubated overnight with primary antibody rotating at 4°C. The membranes were washed with 1x TBST, incubated with secondary antibody for 45 min at 4°C, followed by room temperature for 1 hour, and then washed with 1x TBST. Signals were detected by luminescence using Pierce ECL (Thermo Fisher Scientific, #32209) and a ChemiDoc Imaging System (Bio-Rad). Blots were quantified using the Analyze gels program in FIJI/ImageJ.

xCELLigence Proliferation Assay

16 well E-plates (Agilent, # 300 600 890) were used for the experiment on an Agilent xCELLigence Real Time Cell Analysis (RTCA) Dual Purpose (DP) machine and RTCA Basic software (Agilent). Pre-warmed media was added to each well and used to take a background measurement for 1 minute. Cells were grown until 80% confluency, washed with 1xPBS, trypsinized, centrifuged at 1000 rpm for 5 min and then resuspended in cell culture media for a manual cell count using trypan blue. 20,000 cells/well were then plated for each cell line in a volume of 100 µl/well for a total volume of 150 µl/well. Each plate included blank wells with 150 µl of media for a negative control. Cells were allowed to settle

450 and attach to the plate at room temperature in the cell culture hood for 30 minutes, after which the plate
451 was inserted into the machine. The Xcelligence machine was set to take a measurement every hour
452 for 48 hours. The experiment was completed with n = 3 biological replicates and 4 technical replicates
453 per cell line. Results were exported from the RTCA software and graphical displays were made in Prism
454 10 (Graphpad). The cell index from each run was normalized to the final end point of the Caco2 WT
455 cell line to determine fold change and a two-way ANOVA with Greenhouse–Geisser correction and
456 Bonferroni correction.
457

458 **Low Attachment (Anchorage-Independent Growth) Assay**

459 Cells were trypisinzed with 0.25% Trypsin-EDTA (Gibco, #25200-056) and counted using a manual cell
460 count and trypan blue (Corning, #25-900-CI). Cells were then suspended in culture media appropriate
461 for the cell line that contained 2.5% basement membrane substrate (Cultrex Basement Membrane
462 Extract, Pathclear, #3432-001-01) and plated on an ultra-low attachment 96-well plate (Corning, #3474)
463 at a seeding density of 1000 cells per well. Plates were cultured for a total of 10 days, adding 50 ul of
464 media to the wells every other day and were fixed using 4% paraformaldehyde (PFA) (Electron
465 Microscopy Sciences, # 157-4) diluted to a final concentration of 1% PFA. The experiment was
466 completed with n = 4 biological replicates and 9 technical replicates per cell line. Following fixation,
467 plates were imaged on a Keyence BZ-X810 microscope. Images were analyzed in FIJI/ImageJ utilizing
468 the BioVoxxel Toolbox Plugin v2.6.0, thresholding and using the analyze particles function to measure
469 the area, perimeter, Feret's diameter, and circularity of the spheroids(Brocher).
470

471 **LINE1 Reporter Assay**

472 The LINE1 reporter constructs used in this study were a gift from Eline Luning Prak. The plasmids used
473 in this study contain the indicated modifications to the pCEP4 vector backbone as previously
474 described(Moran et al., 1996, Ostertag et al., 2000, Garcia-Perez et al., 2010, Kopera et al., 2016). In
475 detail:

476 *pCEP4puroeGFP* (pCEP4+) The vector backbone is the pCEP4 plasmid with the hygromycin
477 resistance gene replaced with puromycin for selection. It contains the coding sequence for enhanced
478 GFP (eGFP) and constitutively expresses eGFP with puromycin selection. This is the positive control
479 for the retrotransposition assay and is used to determine the transfection efficiency (Addgene
480 #177922).

481 *pJM111L1eGFP (LINE1 inactive)* The vector backbone is the pCEP4 plasmid with the hygromycin
482 resistance gene replaced with puromycin for selection. This vector contains a retro-transposition
483 defective allele of LINE1 that contains two missense mutations ($RR_{261-262}AA$) in the LINE1 ORF1-

484 encoded protein (ORF1p) and also contains the eGFP indicator cassette. This plasmid cannot express
485 eGFP and is a negative control for the retro-transposition assay (Addgene #42941).
486 *p99LINE1RP-GFP (LINE1-GFP reporter)* The vector backbone is the pCEP4 plasmid with the
487 hygromycin resistance gene replaced with puromycin for selection. This vector lacks the CMV promoter
488 and contains a full-length retro-transposition competent LINE1 element and the eGFP indicator
489 cassette subcloned into the 3'UTR of LINE1 (Addgene #42940).
490 Caco2 wild type or PIWIL2 KO cells were seeded onto 18mm circular glass coverslips in 12 well plates
491 for immunofluorescence staining and allowed to grow until 70% confluency. Cells were transfected
492 using Lipofectamine 3000 (Thermo Fisher #L3000-001) according to manufacturer's instructions with
493 1µg of pCEP4puroeGFP, or 1µg pJM111L1eGFP or 1µg p99LINE1RP-GFP(Day 0). 16 hours post
494 transfection, the media was changed with fresh cell culture media (Day 1). At 48 hours post-transfection,
495 cells were placed in puromycin selection at a concentration of 5 µg/ml (Day 2). 48 hours later, media
496 was changed with fresh, and cells were kept in puromycin selection (Day 4). After 4 days of puromycin
497 selection (Day 6 post-transfection), the cells were then fixed with 4% paraformaldehyde, washed with
498 1xPBS with 10mM glycine followed by permeabilization with 0.02% Triton-X 100 and stained with DAPI.
499 Three fields per condition were captured and the experiment was completed with n = 4 biological
500 replicates and imaged using a Keyence BZ-X810 microscope. Images were analyzed by FIJI/ImageJ.
501 The average number of retro-transposition events was divided by the transfection efficiency of the
502 pCEP4+ positive control plasmid and then normalized to the L1 inactive plasmid for each cell line.
503
504 **Immunofluorescence**
505 Cells were grown in 12-well plates on 18 mm circular sterile glass coverslips (Fisher Scientific #72222-
506 01) until they reached 80% confluency. Cells were washed once with 1x PBS and fixed with 100%
507 methanol (Thermo Fisher Scientific) at –20°C for 7 min followed by 1x PBS wash. Coverslips were then
508 blocked with serum free Protein Block reagent (Dako, #X0909) at RT for 1hr and stained with primary
509 antibodies diluted in Antibody Diluent (Dako, #S3022) as described in the antibodies table overnight at
510 4°C. Cells were then washed with 1x PBS and stained with the fluorescent-labeled secondary
511 antibodies for 1 hour at room temperature. Coverslips were then washed with 1x PBS, co-stained with
512 DAPI (Sigma-Aldrich, #D8417) and mounted with Aqua-Poly/Mount (Polysciences, #18606-20).
513
514 **Confocal Imaging and Image processing**
515 Confocal images of γH2AX foci were acquired using a Leica SP8 confocal microscope with a 63x Plan-
516 Apochromat 1.4NA DIC oil immersion objective (Leica) and 405 nm and 633 nm lasers. Image
517 acquisition was completed using the Leica Application Suite software at 2048 × 2048 resolution and
518 with 0.3 µm intervals along the z-axis. The same imaging parameters were used across conditions for

each set of experiments to allow for comparisons. Z-stacks of all samples were analyzed using the FIJI/ImageJ analysis software and a max projection of each image was used to visualize the nucleus and account for uneven cell thickness over the entire field. Three fields of each sample were captured, and the experiment was performed in n = 3 biological replicates. Total γH2AX foci were quantified by thresholding the images and using the analyze particles function, then normalized to the total number of cells in the field. Nuclei on the borders were excluded from the cell count calculation in FIJI.

Analysis and Statistics

For all measurements, sample size and related statistics are indicated in the respected figure legends and were analyzed and graphed using Prism 10 (GraphPad). All experiments were performed in at least three independent experiments, unless otherwise noted, with alpha = 0.05 and representative images are shown. Statistical tests are noted in each figure legend along with p-values. For tests that required multiple comparisons, the multiplicity adjusted p-value is reported.

ACKNOWLEDGMENTS

We would like to thank Drs. Christiana Kappler and Stephen Duncan, Cell Models Core, Medical University of South Carolina Center of Biomedical Research Excellence (COBRE) in Digestive & Liver Disease (CDLD; National Institutes of Health P20 GM130457) for support with CRISPR/Cas9 reagents.

COMPETING INTERESTS

No competing interests declared.

FUNDING

This work was supported by National Institute of Health grants R01 DK124553, R01 DK136658, R21 CA246233, P20 GM130457 (COBRE in Digestive & Liver Disease, MUSC), P30 DK123704 (Digestive Disease Research Center, MUSC), to AK; R01 GM160815 to VG; and DP2 CA280626 to JRD. A.R. was supported by National Institutes of Health training grants TL1 TR001451, UL1 TR001450, T32 5T32DK124191, and 1F31DK138780-01.

REFERENCES

ARIUMI, Y. 2016. Guardian of the Human Genome: Host Defense Mechanisms against LINE-1 Retrotransposition. *Front Chem,* 4**,** 28.

BECK, C. R., COLLIER, P., MACFARLANE, C., MALIG, M., KIDD, J. M., EICHLER, E. E., BADGE, R. M. & MORAN, J. V. 2010. LINE-1 retrotransposition activity in human genomes. *Cell,* 141**,** 1159-70.

BECK, C. R., GARCIA-PEREZ, J. L., BADGE, R. M. & MORAN, J. V. 2011. LINE-1 elements in structural variation and disease. *Annu Rev Genomics Hum Genet,* 12**,** 187-215.

BERRENS, R. V., ANDREWS, S., SPENSBERGER, D., SANTOS, F., DEAN, W., GOULD, P., SHARIF, J., OLOVA, N., CHANDRA, T., KOSEKI, H., VON MEYENN, F. & REIK, W. 2017. An endosiRNA-Based Repression Mechanism Counteracts Transposon Activation during Global DNA Demethylation in Embryonic Stem Cells. *Cell Stem Cell,* 21**,** 694-703 e7.

BOWERS, R. R., JONES, C. M., PAZ, E. A., BARROWS, J. K., ARMESON, K. E., LONG, D. T. & DELANEY, J. R. 2022. SWAN pathway-network identification of common aneuploidy-based oncogenic drivers. *Nucleic Acids Res,* 50**,** 3673-3692.

BROCHER, J. BioVoxxel Toolbox. v2.6.0 ed.

CAJUSO, T., SULO, P., TANSKANEN, T., KATAINEN, R., TAIRA, A., HANNINEN, U. A., KONDELIN, J., FORSSTROM, L., VALIMAKI, N., AAVIKKO, M., KAASINEN, E., RISTIMAKI, A., KOSKENSALO, S., LEPISTO, A., RENKONEN-SINISALO, L., SEPPALA, T., KUOPIO, T., BOHM, J., MECKLIN, J. P., KILPIVAARA, O., PITKANEN, E., PALIN, K. & AALTONEN, L. A. 2019. Retrotransposon insertions can initiate colorectal cancer and are associated with poor survival. *Nat Commun,* 10**,** 4022.

CERAMI, E., GAO, J., DOGRUSOZ, U., GROSS, B. E., SUMER, S. O., AKSOY, B. A., JACOBSEN, A., BYRNE, C. J., HEUER, M. L., LARSSON, E., ANTIPIN, Y., REVA, B., GOLDBERG, A. P., SANDER, C. & SCHULTZ, N. 2012. The cBio cancer genomics portal: an open platform for exploring multidimensional cancer genomics data. *Cancer Discov,* 2**,** 401-4.

CHANDRASHEKAR, D. S., BASHEL, B., BALASUBRAMANYA, S. A. H., CREIGHTON, C. J., PONCE-RODRIGUEZ, I., CHAKRAVARTHI, B. & VARAMBALLY, S. 2017. UALCAN: A Portal for Facilitating Tumor Subgroup Gene Expression and Survival Analyses. *Neoplasia,* 19**,** 649-658.

CHANDRASHEKAR, D. S., KARTHIKEYAN, S. K., KORLA, P. K., PATEL, H., SHOVON, A. R., ATHAR, M., NETTO, G. J., QIN, Z. S., KUMAR, S., MANNE, U., CREIGHTON, C. J. & VARAMBALLY, S. 2022. UALCAN: An update to the integrated cancer data analysis platform. *Neoplasia,* 25**,** 18-27.

DAULAGALA, A. C., CETIN, M., NAIR-MENON, J., JIMENEZ, D. W., BRIDGES, M. C., BRADSHAW, A. D., SAHIN, O. & KOURTIDIS, A. 2024. The epithelial adherens junction component PLEKHA7 regulates ECM remodeling and cell behavior through miRNA-mediated regulation of MMP1 and LOX. *bioRxiv 10.1101/2024.05.28.596237*.

DE BRUIJN, I., KUNDRA, R., MASTROGIACOMO, B., TRAN, T. N., SIKINA, L., MAZOR, T., LI, X., OCHOA, A., ZHAO, G., LAI, B., ABESHOUSE, A., BAICEANU, D., CIFTCI, E., DOGRUSOZ, U., DUFILIE, A., ERKOC, Z., GARCIA LARA, E., FU, Z., GROSS, B., HAYNES, C., HEATH, A., HIGGINS, D., JAGANNATHAN, P., KALLETLA, K., KUMARI, P., LINDSAY, J., LISMAN, A., LEENKNEGT, B., LUKASSE, P., MADELA, D., MADUPURI, R., VAN NIEROP, P., PLANTALECH, O., QUACH, J., RESNICK, A. C., RODENBURG, S. Y. A., SATRAVADA, B. A., SCHAEFFER, F., SHERIDAN, R., SINGH, J., SIROHI, R., SUMER, S. O., VAN HAGEN, S., WANG, A., WILSON, M., ZHANG, H., ZHU, K., RUSK, N., BROWN, S., LAVERY, J. A., PANAGEAS, K. S., RUDOLPH, J. E., LENOUE-NEWTON, M. L., WARNER, J. L., GUO, X., HUNTER-ZINCK, H., YU, T. V., PILAI, S., NICHOLS, C., GARDOS, S. M., PHILIP, J., AACR PROJECT GENIE BPC CORE TEAM, A. P. G. C., KEHL, K. L., RIELY, G. J., SCHRAG, D., LEE, J., FIANDALO, M. V., SWEENEY, S. M., PUGH, T. J., SANDER, C., CERAMI, E., GAO, J. & SCHULTZ, N. 2023. Analysis and Visualization of Longitudinal Genomic and Clinical Data from the AACR Project GENIE Biopharma Collaborative in cBioPortal. *Cancer Res,* 83**,** 3861-3867.

DE FAZIO, S., BARTONICEK, N., DI GIACOMO, M., ABREU-GOODGER, C., SANKAR, A., FUNAYA, C., ANTONY, C., MOREIRA, P. N., ENRIGHT, A. J. & O'CARROLL, D. 2011. The endonuclease activity of Mili fuels piRNA amplification that silences LINE1 elements. *Nature,* 480**,** 259-63.

ECKSTEIN, M., JUNG, R., WEIGELT, K., SIKIC, D., STOHR, R., GEPPERT, C., AGAIMY, A., LIEB, V., HARTMANN, A., WULLICH, B., WACH, S. & TAUBERT, H. 2018. Piwi-like 1 and -2 protein expression levels are prognostic factors for muscle invasive urothelial bladder cancer patients. *Sci Rep,* 8**,** 17693.

598 ELBARBARY, R. A., LUCAS, B. A. & MAQUAT, L. E. 2016. Retrotransposons as regulators of gene expression.
599 *Science,* 351**,** aac7247.
600 EWING, A. D., GACITA, A., WOOD, L. D., MA, F., XING, D., KIM, M. S., MANDA, S. S., ABRIL, G., PEREIRA, G.,
601 MAKOHON-MOORE, A., LOOIJENGA, L. H., GILLIS, A. J., HRUBAN, R. H., ANDERS, R. A., ROMANS, K. E.,
602 PANDEY, A., IACOBUZIO-DONAHUE, C. A., VOGELSTEIN, B., KINZLER, K. W., KAZAZIAN, H. H., JR. &
603 SOLYOM, S. 2015. Widespread somatic L1 retrotransposition occurs early during gastrointestinal cancer
604 evolution. *Genome Res,* 25**,** 1536-45.
605 FLEMING, M., RAVULA, S., TATISHCHEV, S. F. & WANG, H. L. 2012. Colorectal carcinoma: Pathologic aspects. *J*
606 *Gastrointest Oncol,* 3**,** 153-73.
607 FROST, R. J., HAMRA, F. K., RICHARDSON, J. A., QI, X., BASSEL-DUBY, R. & OLSON, E. N. 2010. MOV10L1 is
608 necessary for protection of spermatocytes against retrotransposons by Piwi-interacting RNAs. *Proc Natl*
609 *Acad Sci U S A,* 107**,** 11847-52.
610 FU, K., TIAN, S., TAN, H., WANG, C., WANG, H., WANG, M., WANG, Y., CHEN, Z., WANG, Y., YUE, Q., XU, Q., ZHANG,
611 S., LI, H., XIE, J., LIN, M., LUO, M., CHEN, F., YE, L. & ZHENG, K. 2019. Biological and RNA regulatory
612 function of MOV10 in mammalian germ cells. *BMC Biol,* 17**,** 39.
613 GAO, J., AKSOY, B. A., DOGRUSOZ, U., DRESDNER, G., GROSS, B., SUMER, S. O., SUN, Y., JACOBSEN, A., SINHA,
614 R., LARSSON, E., CERAMI, E., SANDER, C. & SCHULTZ, N. 2013. Integrative analysis of complex cancer
615 genomics and clinical profiles using the cBioPortal. *Sci Signal,* 6**,** pl1.
616 GAO, J., JING, J., SHANG, G., CHEN, C., DUAN, M., YU, W., WANG, K., LUO, J., SONG, M., CHEN, K., CHEN, C.,
617 ZHANG, T. & DING, D. 2024. TDRD1 phase separation drives intermitochondrial cement assembly to
618 promote piRNA biogenesis and fertility. *Dev Cell,* 59**,** 2704-2718 e6.
619 GAO, J. X. 2008. Cancer stem cells: the lessons from pre-cancerous stem cells. *J Cell Mol Med,* 12**,** 67-96.
620 GARCIA-PEREZ, J. L., MORELL, M., SCHEYS, J. O., KULPA, D. A., MORELL, S., CARTER, C. C., HAMMER, G. D.,
621 COLLINS, K. L., O'SHEA, K. S., MENENDEZ, P. & MORAN, J. V. 2010. Epigenetic silencing of engineered L1
622 retrotransposition events in human embryonic carcinoma cells. *Nature,* 466**,** 769-73.
623 GASIOR, S. L., WAKEMAN, T. P., XU, B. & DEININGER, P. L. 2006. The human LINE-1 retrotransposon creates DNA
624 double-strand breaks. *J Mol Biol,* 357**,** 1383-93.
625 GORDON, I. O., AGRAWAL, N., WILLIS, E., GOLDBLUM, J. R., LOPEZ, R., ALLENDE, D., LIU, X., PATIL, D. Y., YERIAN,
626 L., EL-KHIDER, F., FIOCCHI, C. & RIEDER, F. 2018. Fibrosis in ulcerative colitis is directly linked to severity
627 and chronicity of mucosal inflammation. *Aliment Pharmacol Ther,* 47**,** 922-939.
628 GRANDI, F. C. & AN, W. 2013. Non-LTR retrotransposons and microsatellites: Partners in genomic variation. *Mob*
629 *Genet Elements,* 3**,** e25674.
630 GRASSET, E., PINTO, M., DUSSAULX, E., ZWEIBAUM, A. & DESJEUX, J. F. 1984. Epithelial properties of human
631 colonic carcinoma cell line Caco-2: electrical parameters. *Am J Physiol,* 247**,** C260-7.
632 GUIDOBONI, M., GAFA, R., VIEL, A., DOGLIONI, C., RUSSO, A., SANTINI, A., DEL TIN, L., MACRI, E., LANZA, G.,
633 BOIOCCHI, M. & DOLCETTI, R. 2001. Microsatellite instability and high content of activated cytotoxic
634 lymphocytes identify colon cancer patients with a favorable prognosis. *Am J Pathol,* 159**,** 297-304.
635 GYORFFY, B. 2024. Integrated analysis of public datasets for the discovery and validation of survival-associated
636 genes in solid tumors. *Innovation (Camb),* 5**,** 100625.
637 HAN, B. W., WANG, W., LI, C., WENG, Z. & ZAMORE, P. D. 2015. Noncoding RNA. piRNA-guided transposon
638 cleavage initiates Zucchini-dependent, phased piRNA production. *Science,* 348**,** 817-21.
639 HANAHAN, D. & WEINBERG, R. A. 2011. Hallmarks of cancer: the next generation. *Cell,* 144**,** 646-74.
640 HANCKS, D. C. & KAZAZIAN, H. H., JR. 2016. Roles for retrotransposon insertions in human disease. *Mob DNA,* 7**,**
641 9.
642 HE, G., CHEN, L., YE, Y., XIAO, Y., HUA, K., JARJOURA, D., NAKANO, T., BARSKY, S. H., SHEN, R. & GAO, J. X. 2010.
643 Piwil2 expressed in various stages of cervical neoplasia is a potential complementary marker for p16. *Am J*
644 *Transl Res,* 2**,** 156-69.
645 HIDALGO, I. J., RAUB, T. J. & BORCHARDT, R. T. 1989. Characterization of the human colon carcinoma cell line
646 (Caco-2) as a model system for intestinal epithelial permeability. *Gastroenterology,* 96**,** 736-49.
647 HUANG, A., YANG, Y., SHI, J. Y., LI, Y. K., XU, J. X., CHENG, Y. & GU, J. 2021. Mucinous adenocarcinoma: A unique
648 clinicopathological subtype in colorectal cancer. *World J Gastrointest Surg,* 13**,** 1567-1583.

IKEDA, S., TANAKA, K., OHTANI, R., KANDA, A., SOTOMARU, Y., KONO, T. & OBATA, Y. 2022. Disruption of piRNA machinery by deletion of ASZ1/GASZ results in the expression of aberrant chimeric transcripts in gonocytes. *J Reprod Dev,* 68**,** 125-136.

JACOBS, D. I., QIN, Q., LERRO, M. C., FU, A., DUBROW, R., CLAUS, E. B., DEWAN, A. T., WANG, G., LIN, H. & ZHU, Y. 2016. PIWI-Interacting RNAs in Gliomagenesis: Evidence from Post-GWAS and Functional Analyses. *Cancer Epidemiol Biomarkers Prev,* 25**,** 1073-80.

JANG, H. S., SHAH, N. M., DU, A. Y., DAILEY, Z. Z., PEHRSSON, E. C., GODOY, P. M., ZHANG, D., LI, D., XING, X., KIM, S., O'DONNELL, D., GORDON, J. I. & WANG, T. 2019. Transposable elements drive widespread expression of oncogenes in human cancers. *Nat Genet,* 51**,** 611-617.

KANKE, M., KENNEDY NG, M. M., CONNELLY, S., SINGH, M., SCHANER, M., SHANAHAN, M. T., WOLBER, E. A., BEASLEY, C., LIAN, G., JAIN, A., LONG, M. D., BARNES, E. L., HERFARTH, H. H., ISAACS, K. L., HANSEN, J. J., KAPADIA, M., GUILLEM, J. G., FESCHOTTE, C., FUREY, T. S., SHEIKH, S. Z. & SETHUPATHY, P. 2022. Single-Cell Analysis Reveals Unexpected Cellular Changes and Transposon Expression Signatures in the Colonic Epithelium of Treatment-Naive Adult Crohn's Disease Patients. *Cell Mol Gastroenterol Hepatol,* 13**,** 1717-1740.

KIM, E. R. & CHANG, D. K. 2014. Colorectal cancer in inflammatory bowel disease: the risk, pathogenesis, prevention and diagnosis. *World J Gastroenterol,* 20**,** 9872-81.

KIM, K. H., KANG, Y. J., JO, J. O., OCK, M. S., MOON, S. H., SUH, D. S., YOON, M. S., PARK, E. S., JEONG, N., EO, W. K., KIM, H. Y. & CHA, H. J. 2014. DDX4 (DEAD box polypeptide 4) colocalizes with cancer stem cell marker CD133 in ovarian cancers. *Biochem Biophys Res Commun,* 447**,** 315-22.

KISHANI FARAHANI, R., SOLEIMANPOUR, S., GOLMOHAMMADI, M. & SOLEIMANPOUR-LICHAEI, H. R. 2023. PIWIL2 Regulates the Proliferation, Apoptosis and Colony Formation of Colorectal Cancer Cell Line. *Iran J Biotechnol,* 21**,** e3176.

KOPERA, H. C., LARSON, P. A., MOLDOVAN, J. B., RICHARDSON, S. R., LIU, Y. & MORAN, J. V. 2016. LINE-1 Cultured Cell Retrotransposition Assay. *Methods Mol Biol,* 1400**,** 139-56.

KOURTIDIS, A., NGOK, S. P., PULIMENO, P., FEATHERS, R. W., CARPIO, L. R., BAKER, T. R., CARR, J. M., YAN, I. K., BORGES, S., PEREZ, E. A., STORZ, P., COPLAND, J. A., PATEL, T., THOMPSON, E. A., CITI, S. & ANASTASIADIS, P. Z. 2015. Distinct E-cadherin-based complexes regulate cell behaviour through miRNA processing or Src and p120 catenin activity. *Nat Cell Biol,* 17**,** 1145-57.

KU, H. Y. & LIN, H. 2014. PIWI proteins and their interactors in piRNA biogenesis, germline development and gene expression. *Natl Sci Rev,* 1**,** 205-218.

KUO, L. J. & YANG, L. X. 2008. Gamma-H2AX - a novel biomarker for DNA double-strand breaks. *In Vivo,* 22**,** 305-9.

KURAMOCHI-MIYAGAWA, S., WATANABE, T., GOTOH, K., TOTOKI, Y., TOYODA, A., IKAWA, M., ASADA, N., KOJIMA, K., YAMAGUCHI, Y., IJIRI, T. W., HATA, K., LI, E., MATSUDA, Y., KIMURA, T., OKABE, M., SAKAKI, Y., SASAKI, H. & NAKANO, T. 2008. DNA methylation of retrotransposon genes is regulated by Piwi family members MILI and MIWI2 in murine fetal testes. *Genes Dev,* 22**,** 908-17.

LEE, E., LOKMAN, N. A., OEHLER, M. K., RICCIARDELLI, C. & GRUTZNER, F. 2020. A Comprehensive Molecular and Clinical Analysis of the piRNA Pathway Genes in Ovarian Cancer. *Cancers (Basel),* 13.

LEE, J. H., SCHUTTE, D., WULF, G., FUZESI, L., RADZUN, H. J., SCHWEYER, S., ENGEL, W. & NAYERNIA, K. 2006. Stem-cell protein Piwil2 is widely expressed in tumors and inhibits apoptosis through activation of Stat3/Bcl-XL pathway. *Hum Mol Genet,* 15**,** 201-11.

LI, Y., ZHANG, Y. & LIU, M. 2021. Knockout Gene-Based Evidence for PIWI-Interacting RNA Pathway in Mammals. *Front Cell Dev Biol,* 9**,** 681188.

LINGGI, B., JAIRATH, V., ZOU, G., SHACKELTON, L. M., MCGOVERN, D. P. B., SALAS, A., VERSTOCKT, B., SILVERBERG, M. S., NAYERI, S., FEAGAN, B. G. & VANDE CASTEELE, N. 2021. Meta-analysis of gene expression disease signatures in colonic biopsy tissue from patients with ulcerative colitis. *Sci Rep,* 11**,** 18243.

LIU, J. J., SHEN, R., CHEN, L., YE, Y., HE, G., HUA, K., JARJOURA, D., NAKANO, T., RAMESH, G. K., SHAPIRO, C. L., BARSKY, S. H. & GAO, J. X. 2010. Piwil2 is expressed in various stages of breast cancers and has the potential to be used as a novel biomarker. *Int J Clin Exp Pathol,* 3**,** 328-37.

LU, Y., ZHANG, K., LI, C., YAO, Y., TAO, D., LIU, Y., ZHANG, S. & MA, Y. 2012. Piwil2 suppresses p53 by inducing phosphorylation of signal transducer and activator of transcription 3 in tumor cells. *PLoS One,* 7**,** e30999.

LUO, C., CEN, S., DING, G. & WU, W. 2019. Mucinous colorectal adenocarcinoma: clinical pathology and treatment options. *Cancer Commun (Lond),* 39**,** 13.

MA, L., BUCHOLD, G. M., GREENBAUM, M. P., ROY, A., BURNS, K. H., ZHU, H., HAN, D. Y., HARRIS, R. A., COARFA, C., GUNARATNE, P. H., YAN, W. & MATZUK, M. M. 2009. GASZ is essential for male meiosis and suppression of retrotransposon expression in the male germline. *PLoS Genet,* 5**,** e1000635.

MARTINEZ, V. D., VUCIC, E. A., THU, K. L., HUBAUX, R., ENFIELD, K. S., PIKOR, L. A., BECKER-SANTOS, D. D., BROWN, C. J., LAM, S. & LAM, W. L. 2015. Unique somatic and malignant expression patterns implicate PIWI-interacting RNAs in cancer-type specific biology. *Sci Rep,* 5**,** 10423.

MATHIOUDAKIS, N., PALENCIA, A., KADLEC, J., ROUND, A., TRIPSIANES, K., SATTLER, M., PILLAI, R. S. & CUSACK, S. 2012. The multiple Tudor domain-containing protein TDRD1 is a molecular scaffold for mouse Piwi proteins and piRNA biogenesis factors. *RNA,* 18**,** 2056-72.

MESEURE, D., VACHER, S., BOUDJEMAA, S., LAE, M., NICOLAS, A., LECLERE, R., CHEMLALI, W., CHAMPENOIS, G., SCHNITZLER, A., LESAGE, L., DUBOIS, T. & BIECHE, I. 2020. Biopathological Significance of PIWI-piRNA Pathway Deregulation in Invasive Breast Carcinomas. *Cancers (Basel),* 12.

MIKI, Y., NISHISHO, I., HORII, A., MIYOSHI, Y., UTSUNOMIYA, J., KINZLER, K. W., VOGELSTEIN, B. & NAKAMURA, Y. 1992. Disruption of the APC gene by a retrotransposal insertion of L1 sequence in a colon cancer. *Cancer Res,* 52**,** 643-5.

MORAN, J. V., HOLMES, S. E., NAAS, T. P., DEBERARDINIS, R. J., BOEKE, J. D. & KAZAZIAN, H. H., JR. 1996. High frequency retrotransposition in cultured mammalian cells. *Cell,* 87**,** 917-27.

NAM, C. H., YOUK, J., KIM, J. Y., LIM, J., PARK, J. W., OH, S. A., LEE, H. J., PARK, J. W., WON, H., LEE, Y., JEONG, S. Y., LEE, D. S., OH, J. W., HAN, J., LEE, J., KWON, H. W., KIM, M. J. & JU, Y. S. 2023. Widespread somatic L1 retrotransposition in normal colorectal epithelium. *Nature,* 617**,** 540-547.

NISHIMASU, H., ISHIZU, H., SAITO, K., FUKUHARA, S., KAMATANI, M. K., BONNEFOND, L., MATSUMOTO, N., NISHIZAWA, T., NAKANAGA, K., AOKI, J., ISHITANI, R., SIOMI, H., SIOMI, M. C. & NUREKI, O. 2012. Structure and function of Zucchini endoribonuclease in piRNA biogenesis. *Nature,* 491**,** 284-7.

OLOTU, O., KOSKENNIEMI, A. R., MA, L., PARAMONOV, V., LAASANEN, S., LOURAMO, E., BOURGERY, M., LEHTINIEMI, T., LAASANEN, S., RIVERO-MULLER, A., LOYTTYNIEMI, E., SAHLGREN, C., WESTERMARCK, J., VENTELA, S., VISAKORPI, T., POUTANEN, M., VAINIO, P., MAKELA, J. A. & KOTAJA, N. 2024. Germline-specific RNA helicase DDX4 forms cytoplasmic granules in cancer cells and promotes tumor growth. *Cell Rep,* 43**,** 114430.

OSTERTAG, E. M., PRAK, E. T., DEBERARDINIS, R. J., MORAN, J. V. & KAZAZIAN, H. H., JR. 2000. Determination of L1 retrotransposition kinetics in cultured cells. *Nucleic Acids Res,* 28**,** 1418-23.

PANDEY, R. R., TOKUZAWA, Y., YANG, Z., HAYASHI, E., ICHISAKA, T., KAJITA, S., ASANO, Y., KUNIEDA, T., SACHIDANANDAM, R., CHUMA, S., YAMANAKA, S. & PILLAI, R. S. 2013. Tudor domain containing 12 (TDRD12) is essential for secondary PIWI interacting RNA biogenesis in mice. *Proc Natl Acad Sci U S A,* 110**,** 16492-7.

PENG, J. C. & LIN, H. 2013. Beyond transposons: the epigenetic and somatic functions of the Piwi-piRNA mechanism. *Curr Opin Cell Biol,* 25**,** 190-4.

PITKANEN, E., CAJUSO, T., KATAINEN, R., KAASINEN, E., VALIMAKI, N., PALIN, K., TAIPALE, J., AALTONEN, L. A. & KILPIVAARA, O. 2014. Frequent L1 retrotranspositions originating from TTC28 in colorectal cancer. *Oncotarget,* 5**,** 853-9.

RAMAT, A. & SIMONELIG, M. 2021. Functions of PIWI Proteins in Gene Regulation: New Arrows Added to the piRNA Quiver. *Trends Genet,* 37**,** 188-200.

RAN, F. A., HSU, P. D., WRIGHT, J., AGARWALA, V., SCOTT, D. A. & ZHANG, F. 2013. Genome engineering using the CRISPR-Cas9 system. *Nat Protoc,* 8**,** 2281-2308.

REUTER, M., CHUMA, S., TANAKA, T., FRANZ, T., STARK, A. & PILLAI, R. S. 2009. Loss of the Mili-interacting Tudor domain-containing protein-1 activates transposons and alters the Mili-associated small RNA profile. *Nat Struct Mol Biol,* 16**,** 639-46.

RODRIGUEZ-MARTIN, B., ALVAREZ, E. G., BAEZ-ORTEGA, A., ZAMORA, J., SUPEK, F., DEMEULEMEESTER, J., SANTAMARINA, M., JU, Y. S., TEMES, J., GARCIA-SOUTO, D., DETERING, H., LI, Y., RODRIGUEZ-CASTRO, J., DUESO-BARROSO, A., BRUZOS, A. L., DENTRO, S. C., BLANCO, M. G., CONTINO, G., ARDELJAN, D., TOJO, M., ROBERTS, N. D., ZUMALAVE, S., EDWARDS, P. A., WEISCHENFELDT, J., PUIGGROS, M., CHONG, Z., CHEN, K., LEE, E. A., WALA, J. A., RAINE, K. M., BUTLER, A., WASZAK, S. M., NAVARRO, F. C. P.,

754 SCHUMACHER, S. E., MONLONG, J., MAURA, F., BOLLI, N., BOURQUE, G., GERSTEIN, M., PARK, P. J.,
755 WEDGE, D. C., BEROUKHIM, R., TORRENTS, D., KORBEL, J. O., MARTINCORENA, I., FITZGERALD, R. C., VAN
756 LOO, P., KAZAZIAN, H. H., BURNS, K. H., GROUP, P. S. V. W., CAMPBELL, P. J., TUBIO, J. M. C. &
757 CONSORTIUM, P. 2020. Pan-cancer analysis of whole genomes identifies driver rearrangements promoted
758 by LINE-1 retrotransposition. *Nat Genet,* 52**,** 306-319.
759 ROSS, R. J., WEINER, M. M. & LIN, H. 2014a. PIWI proteins and PIWI-interacting RNAs in the soma. *Nature,* 505**,**
760 353-359.
761 ROSS, R. J., WEINER, M. M. & LIN, H. 2014b. PIWI proteins and PIWI-interacting RNAs in the soma. *Nature,* 505**,**
762 353-9.
763 SAMBUY, Y., DE ANGELIS, I., RANALDI, G., SCARINO, M. L., STAMMATI, A. & ZUCCO, F. 2005. The Caco-2 cell line as
764 a model of the intestinal barrier: influence of cell and culture-related factors on Caco-2 cell functional
765 characteristics. *Cell Biol Toxicol,* 21**,** 1-26.
766 SAXE, J. P., CHEN, M., ZHAO, H. & LIN, H. 2013. Tdrkh is essential for spermatogenesis and participates in primary
767 piRNA biogenesis in the germline. *EMBO J,* 32**,** 1869-85.
768 SCOTT, E. C., GARDNER, E. J., MASOOD, A., CHUANG, N. T., VERTINO, P. M. & DEVINE, S. E. 2016. A hot L1
769 retrotransposon evades somatic repression and initiates human colorectal cancer. *Genome Res,* 26**,** 745-
770 55.
771 SHI, S., YANG, Z. Z., LIU, S., YANG, F. & LIN, H. 2020. PIWIL1 promotes gastric cancer via a piRNA-independent
772 mechanism. *Proc Natl Acad Sci U S A,* 117**,** 22390-22401.
773 SIEGEL, R. L., GIAQUINTO, A. N. & JEMAL, A. 2024. Cancer statistics, 2024. *CA Cancer J Clin,* 74**,** 12-49.
774 SIGURDSSON, M. I., SMITH, A. V., BJORNSSON, H. T. & JONSSON, J. J. 2012. The distribution of a germline
775 methylation marker suggests a regional mechanism of LINE-1 silencing by the piRNA-PIWI system. *BMC*
776 *Genet,* 13**,** 31.
777 SIOMI, H. & SIOMI, M. C. 2015. RNA. Phased piRNAs tackle transposons. *Science,* 348**,** 756-7.
778 SIOMI, M. C., MANNEN, T. & SIOMI, H. 2010. How does the royal family of Tudor rule the PIWI-interacting RNA
779 pathway? *Genes Dev,* 24**,** 636-46.
780 SIOMI, M. C., SATO, K., PEZIC, D. & ARAVIN, A. A. 2011. PIWI-interacting small RNAs: the vanguard of genome
781 defence. *Nat Rev Mol Cell Biol,* 12**,** 246-58.
782 SOLYOM, S., EWING, A. D., RAHRMANN, E. P., DOUCET, T., NELSON, H. H., BURNS, M. B., HARRIS, R. S., SIGMON,
783 D. F., CASELLA, A., ERLANGER, B., WHEELAN, S., UPTON, K. R., SHUKLA, R., FAULKNER, G. J.,
784 LARGAESPADA, D. A. & KAZAZIAN, H. H., JR. 2012. Extensive somatic L1 retrotransposition in colorectal
785 tumors. *Genome Res,* 22**,** 2328-38.
786 SUN, Y. H., LEE, B. & LI, X. Z. 2022. The birth of piRNAs: how mammalian piRNAs are produced, originated, and
787 evolved. *Mamm Genome,* 33**,** 293-311.
788 TANG, Z., KANG, B., LI, C., CHEN, T. & ZHANG, Z. 2019. GEPIA2: an enhanced web server for large-scale expression
789 profiling and interactive analysis. *Nucleic Acids Res,* 47**,** W556-W560.
790 TUBIO, J. M., LI, Y., JU, Y. S., MARTINCORENA, I., COOKE, S. L., TOJO, M., GUNDEM, G., PIPINIKAS, C. P., ZAMORA,
791 J., RAINE, K., MENZIES, A., ROMAN-GARCIA, P., FULLAM, A., GERSTUNG, M., SHLIEN, A., TARPEY, P. S.,
792 PAPAEMMANUIL, E., KNAPPSKOG, S., VAN LOO, P., RAMAKRISHNA, M., DAVIES, H. R., MARSHALL, J.,
793 WEDGE, D. C., TEAGUE, J. W., BUTLER, A. P., NIK-ZAINAL, S., ALEXANDROV, L., BEHJATI, S., YATES, L. R.,
794 BOLLI, N., MUDIE, L., HARDY, C., MARTIN, S., MCLAREN, S., O'MEARA, S., ANDERSON, E., MADDISON, M.,
795 GAMBLE, S., GROUP, I. B. C., GROUP, I. B. C., GROUP, I. P. C., FOSTER, C., WARREN, A. Y., WHITAKER, H.,
796 BREWER, D., EELES, R., COOPER, C., NEAL, D., LYNCH, A. G., VISAKORPI, T., ISAACS, W. B., VAN'T VEER,
797 L., CALDAS, C., DESMEDT, C., SOTIRIOU, C., APARICIO, S., FOEKENS, J. A., EYFJORD, J. E., LAKHANI, S. R.,
798 THOMAS, G., MYKLEBOST, O., SPAN, P. N., BORRESEN-DALE, A. L., RICHARDSON, A. L., VAN DE VIJVER,
799 M., VINCENT-SALOMON, A., VAN DEN EYNDEN, G. G., FLANAGAN, A. M., FUTREAL, P. A., JANES, S. M.,
800 BOVA, G. S., STRATTON, M. R., MCDERMOTT, U. & CAMPBELL, P. J. 2014. Mobile DNA in cancer. Extensive
801 transduction of nonrepetitive DNA mediated by L1 retrotransposition in cancer genomes. *Science,* 345**,**
802 1251343.
803 UNHAVAITHAYA, Y., HAO, Y., BEYRET, E., YIN, H., KURAMOCHI-MIYAGAWA, S., NAKANO, T. & LIN, H. 2009. MILI, a
804 PIWI-interacting RNA-binding protein, is required for germ line stem cell self-renewal and appears to
805 positively regulate translation. *J Biol Chem,* 284**,** 6507-19.

806 VOUREKAS, A., ZHENG, K., FU, Q., MARAGKAKIS, M., ALEXIOU, P., MA, J., PILLAI, R. S., MOURELATOS, Z. & WANG,
807 P. J. 2015. The RNA helicase MOV10L1 binds piRNA precursors to initiate piRNA processing. *Genes Dev,* 29**,**
808 617-29.
809 WALTER, M., TEISSANDIER, A., PEREZ-PALACIOS, R. & BOURC'HIS, D. 2016. An epigenetic switch ensures
810 transposon repression upon dynamic loss of DNA methylation in embryonic stem cells. *Elife,* 5.
811 WANG, H. L., CHEN, B. B., CAO, X. G., WANG, J., HU, X. F., MU, X. Q. & CHEN, X. B. 2015. The clinical significances
812 of the abnormal expressions of Piwil1 and Piwil2 in colonic adenoma and adenocarcinoma. *Onco Targets*
813 *Ther,* 8**,** 1259-64.
814 WANG, L., NORRIS, E. T. & JORDAN, I. K. 2017. Human Retrotransposon Insertion Polymorphisms Are Associated
815 with Health and Disease via Gene Regulatory Phenotypes. *Front Microbiol,* 8**,** 1418.
816 WANG, Z. Y., GE, L. P., OUYANG, Y., JIN, X. & JIANG, Y. Z. 2024. Targeting transposable elements in cancer:
817 developments and opportunities. *Biochim Biophys Acta Rev Cancer,* 1879**,** 189143.
818 WATANABE, T. & LIN, H. 2014. Posttranscriptional regulation of gene expression by Piwi proteins and piRNAs. *Mol*
819 *Cell,* 56**,** 18-27.
820 WEICK, E. M. & MISKA, E. A. 2014. piRNAs: from biogenesis to function. *Development,* 141**,** 3458-71.
821 WENDA, J. M., HOMOLKA, D., YANG, Z., SPINELLI, P., SACHIDANANDAM, R., PANDEY, R. R. & PILLAI, R. S. 2017.
822 Distinct Roles of RNA Helicases MVH and TDRD9 in PIWI Slicing-Triggered Mammalian piRNA Biogenesis
823 and Function. *Dev Cell,* 41**,** 623-637 e9.
824 XIOL, J., CORA, E., KOGLGRUBER, R., CHUMA, S., SUBRAMANIAN, S., HOSOKAWA, M., REUTER, M., YANG, Z.,
825 BERNINGER, P., PALENCIA, A., BENES, V., PENNINGER, J., SACHIDANANDAM, R. & PILLAI, R. S. 2012. A
826 role for Fkbp6 and the chaperone machinery in piRNA amplification and transposon silencing. *Mol Cell,* 47**,**
827 970-9.
828 YAN, Z., HU, H. Y., JIANG, X., MAIERHOFER, V., NEB, E., HE, L., HU, Y., HU, H., LI, N., CHEN, W. & KHAITOVICH, P.
829 2011. Widespread expression of piRNA-like molecules in somatic tissues. *Nucleic Acids Res,* 39**,** 6596-607.
830 YANG, Z., CHEN, K. M., PANDEY, R. R., HOMOLKA, D., REUTER, M., JANEIRO, B. K., SACHIDANANDAM, R.,
831 FAUVARQUE, M. O., MCCARTHY, A. A. & PILLAI, R. S. 2016. PIWI Slicing and EXD1 Drive Biogenesis of
832 Nuclear piRNAs from Cytosolic Targets of the Mouse piRNA Pathway. *Mol Cell,* 61**,** 138-52.
833 ZENG, G., ZHANG, D., LIU, X., KANG, Q., FU, Y., TANG, B., GUO, W., ZHANG, Y., WEI, G. & HE, D. 2017. Co-
834 expression of Piwil2/Piwil4 in nucleus indicates poor prognosis of hepatocellular carcinoma. *Oncotarget,* 8**,**
835 4607-4617.
836 ZENG, Q., WAN, H., ZHAO, S., XU, H., TANG, T., OWARE, K. A. & QU, S. 2020. Role of PIWI-interacting RNAs on cell
837 survival: Proliferation, apoptosis, and cycle. *IUBMB Life,* 72**,** 1870-1878.
838 ZHANG, X., YU, L., YE, S., XIE, J., HUANG, X., ZHENG, K. & SUN, B. 2019. MOV10L1 Binds RNA G-Quadruplex in a
839 Structure-Specific Manner and Resolves It More Efficiently Than MOV10. *iScience,* 17**,** 36-48.
840 ZHUO, C., LI, Q., WU, Y., LI, Y., NIE, J., LI, D., PENG, J., LIAN, P., LI, B., CAI, G., LI, X. & CAI, S. 2015. LINE-1
841 hypomethylation in normal colon mucosa is associated with poor survival in Chinese patients with
842 sporadic colon cancer. *Oncotarget,* 6**,** 23820-36.

843

844

845 **FIGURE LEGENDS**

846 **Figure 1. The PIWI-piRNA pathway experiences copy number alterations (CNAs) in colon cancer.**
847 Shifted Weighted Annotation Network (SWAN) analysis was performed to interrogate pathway and
848 CNAs within The Cancer Genome Atlas (TCGA) dataset. The Single-pathway SWAN tool was used to
849 perform Gene Ontology Biological Process Analysis on the piRNA metabolic pathway in colon
850 adenocarcinoma (COAD). A) SWAN pathway scoring for each member of the piRNA pathway where
851 blue represents negatively scored allelic losses and red represents positively scored copy number
852 gains within the network (Wilcoxon rank sum $p < 1.7E-10$). B) Circos plot mapping allelic losses (blue)
853 or gains (red) to each respective chromosome. C) Table of the percentages of CNAs for each member
854 of the piRNA pathway ranked by percent biallelic deletions. D) The cBioportal database was used to
855 interrogate TCGA COAD dataset for Overall survival of PIWIL2 allelic loss compared to unaltered
856 tumors. Red indicates PIWIL2 shallow deletions while blue indicates samples with no CNAs. (Logrank
857 Test $p = 0.0204$)

858

859 **Figure 2. PIWIL2 is expressed in normal somatic tissues particularly of gastrointestinal origin.**
860 The UALCAN web-based tool was used to perform a Pan-Cancer analysis of TCGA RNA-seq data to
861 determine PIWIL2 expression across multiple cancer types. Normal samples are indicated in blue and
862 tumor samples are indicated in red. Tumor types queried include: bladder urothelial carcinoma (BLCA),
863 breast invasive carcinoma (BRCA), cervical squamous cell carcinoma and endocervical
864 adenocarcinoma (CESC), cholangiocarcinoma (CHOL), colon adenocarcinoma (COAD), esophageal
865 carcinoma (ESCA), glioblastoma multiforme (GBM), head and neck squamous cell carcinoma (HNSC),
866 kidney chromophobe (KICH), kidney renal clear cell carcinoma (KIRC), kidney renal papillary cell
867 carcinoma (KIRP), liver hepatocellular carcinoma (LIHC), lung adenocarcinoma (LUAD), lung
868 squamous cell carcinoma (LUSC), pancreatic adenocarcinoma (PAAD), prostate adenocarcinoma
869 (PRAD), pheochromocytoma and paraganglioma (PCPG), rectum adenocarcinoma (READ), sarcoma
870 (SARC), skin cutaneous melanoma (SKCM), thyroid carcinoma (THCA), thymoma (THYM), stomach
871 adenocarcinoma (STAD), and uterine corpus endometrial carcinoma (UCEC).

872

873 **Figure 3. PIWIL2 is differentially expressed in colon tumors of advanced stage and nodal**
874 **metastasis, histological subtype, and age.** PIWIL2 expression was queried in the TCGA colon
875 adenocarcinoma (COAD) data set and stratified by comparing normal colon tissue vs A) primary tumor,
876 B) tumor stage, C) tumor nodal metastasis, D) tumor p53 status, E) tumor histological subtype, F) tumor
877 microsatellite stability, as well as G) age, H) weight, I) race and J) biological sex of colon cancer
878 patients. Normal tissues were defined as adjacent non-cancerous tissue. For panels A-E and G-I the
879 UALCAN web-based tool was used to stratify TCGA RNA-seq data for more in-depth analysis of

880 expression profiles. The median and interquartile range is displayed, and *p<0.05, **p<0.01,
881 ***p<0.001. For panel F The GEPIA2 tool was utilized to further stratify PIWIL2 expression in the TCGA
882 COAD dataset by cancer subtype: micro-satellite stable (MSS), micro-satellite instable low (MSI-L), and
883 micro-satellite instable high (MSI-H). The GEPIA2 program calculated statistical significance using one-
884 way ANOVA (*p<0.05). K-L) The Kaplan-Meier Plotter tool was used to determine if PIWIL2 expression
885 impacted patient regression free survival for all stages combined, Stages 1+2+3 and Stage 4.
886
887 **Figure 4. The promoter of PIWIL2 is highly methylated in colon cancer.** PIWIL2 promoter
888 methylation was queried in the TCGA colon adenocarcinoma (COAD) data set and stratified by
889 comparing normal colon tissue vs A) primary tumor, B) tumor stage, C) tumor nodal metastasis, D)
890 tumor p53 status, E) tumor histological subtype, as well as F) biological sex, G) age, H) weight, and I)
891 race of colon cancer patients. Normal tissues were defined as adjacent non-cancerous tissue. The
892 median and interquartile range is displayed, and *p <0.05, **p<0.01, ***p<0.001. A beta value closer to
893 1 indicates higher levels of methylation.
894
895 **Figure 5. PIWIL2 is downregulated in ulcerative colitis patients compared to healthy, non-IBD**
896 **patients.** A meta-analysis of ulcerative colitis tissue gene expression was performed using the
897 PreMedIBD Gene Tool. A) PIWIL2, B) PIWIL4, C) MOV10L1, D) TDRD1, E) TDRD9, F) TDRD12, G)
898 DDX4, H) PLD6 and I) EXD1 were queried and the log_2-fold gene expression changes between
899 ulcerative colitis patients and non-IBD controls were determined for each gene. The meta-analysis was
900 calculated using a random effects model and shows the meta-log2-Fold change and 95% confidence
901 interval. Ulcerative Colitis datasets used are available in the Gene Expression Omnibus: GSE13367,
902 GSE9452, GSE53306, GSE38713, GSE47908, GSE73661, GSE114527, GSE87466 and are
903 represented by grey dots. The summary fold change is displayed with a blue line indicating
904 downregulation, while a positive line indicates upregulation. A log_2-fold-change of 0.5 was used as a
905 threshold for significance.
906
907 **Figure 6. The characterization of PIWIL2 CRISPR KO cells reveals increased spheroid growth**
908 **compared to wild type Caco2 cells.** A) qPCR of PIWIL2 comparing PIWIL2 KO to Caco2 wild type
909 (WT). Data were analyzed and normalized to 18S ribosomal RNA by ΔΔCt calculations to calculate fold
910 change. (n=3 biological replicates, mean ± SE, t-test *p=0.0309). B) Representative western blot of
911 total PIWIL2 and β-actin (Actin) loading control in Caco2 WT and PIWIL2 KO cells. Two bands are
912 visible at the expected molecular weight of full length PIWIL2 of 109 kDa. C) Quantification of the upper
913 band of PIWIL2 by western blot to confirm the knockout (n=3 biological replicates, mean ± SE, t-test
914 **p = 0.0025). D) xCELLigence cellular impedance assay to examine the proliferation rates of Caco2

915 WT and PIWIL2 KO cells in 2-dimensions (2D) (n=3 biological replicates, two-way ANOVA with Geisser-
916 Greenhouse correction and Bonferroni correction for multiple comparisons, Time x Cell Line
917 ****p<0.0001). E) Representative Images of Caco2 WT and PIWIL2 KO cells grown in anchorage
918 independent conditions. F) Area of Caco2 WT and PIWIL2 KO spheroids (***p=0.0001) G) Perimeter
919 of Caco2 WT and PIWIL2 KO spheroids (***p=0.0008) H) Diameter of Caco2 WT and PIWIL2 KO
920 spheroids (***p=0.0005) I) Circularity of Caco2 WT and PIWIL2 KO spheroids (p=0.5041). For the low
921 attachment assay n=4 biological replicates, mean ± SE is displayed, t-test was used for statistical
922 analysis between groups.
923
924 **Figure 7. PIWIL2 depletion increases LINE1 levels and activity.** A) qPCR of L1RE1 comparing
925 PIWIL2 KO to Caco2 WT. Data were analyzed and normalized to 18S ribosomal RNA by ΔΔCt
926 calculations to calculate fold change. (n=3 biological replicates, mean ± SE, t-test *p = 0.0267) B)
927 Representative fluorescent images of Caco2 WT or PIWIL2 KO cells that were transfected with either
928 a constitutively active GFP reporter (pCEP4+), a LINE1 retro-transposition defective reporter (LINE1
929 inactive (-)) or a LINE1-GFP reporter plasmid that expresses GFP only when LINE1 retro-transposition
930 occurs. C) Quantification of the average % positive GFP expressing cells normalized to transfection
931 efficiency for each cell line. (n = 4 biological replicates with 3 fields taken per condition and averaged,
932 mean ± SE, two-way ANOVA with Bonferroni correction for multiple comparisons, PIWIL2 KO LINE1
933 inactive (-) vs. PIWIL2 KO LINE1 GFP *p = 0.0212, Caco2 WT LINE1 inactive (-) vs. PIWIL2 KO
934 LINE1 GFP **p = 0.0076, Caco2 WT LINE1 GFP vs. PIWIL2 KO LINE1 GFP **p = 0.0091).
935
936 **Figure 8. PIWIL2 depletion promotes DNA damage.** A) γH2AX increases in PIWIL2 KO cells
937 compared to Caco2 WT cells by immunofluorescence. Representative confocal images shown B)
938 Quantification of γH2AX foci per cell (n = 9 fields (3 biological replicates, 3 fields per replicate), mean
939 ± SE, t-test *p = 0.0151) C) Representative western blot of total H2AX, phosphorylated γH2AX, and β-
940 actin (Actin) loading control in Caco2 and PIWIL2 KO cells.
941
942 **Supplemental Table 1. PIWI mRNAs in Caco2 cells.** PIWIL2 and PIWIL4 are expressed in Caco2
943 cells. Gene symbol, gene ID and average reads per million (avg rpms) are displayed. n=3 biological
944 replicates.

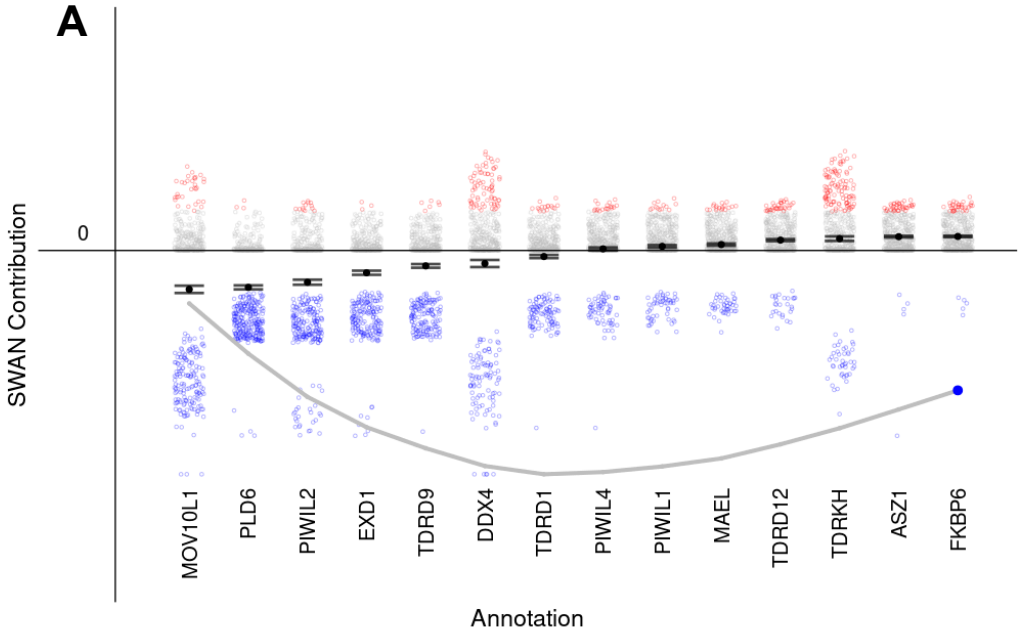

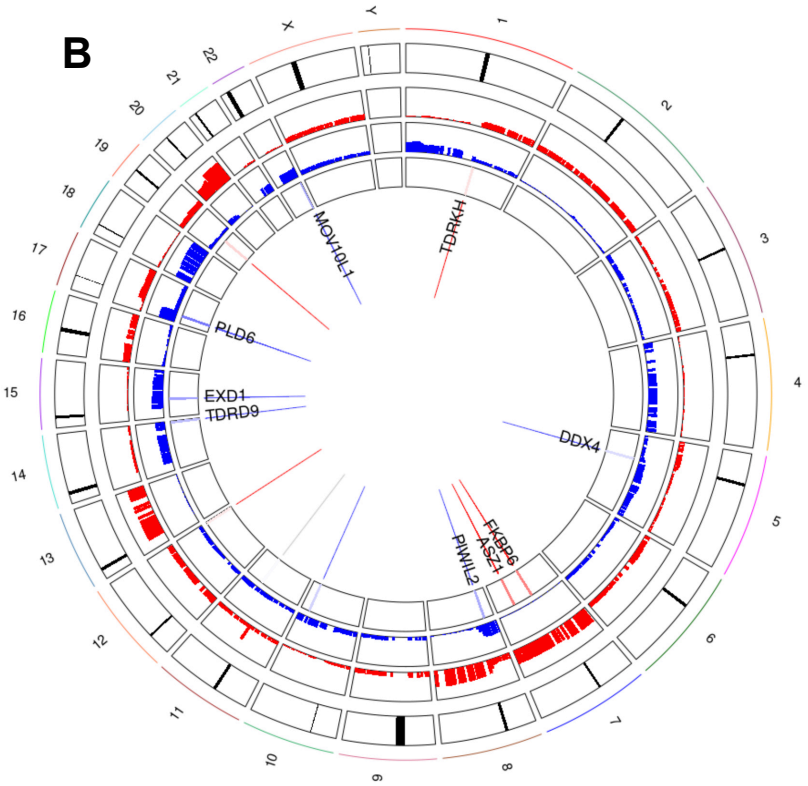

C

Gene	Percent Deleted	Percent Allelic Loss	Percent Normal	Percent Extra Allele	Percent Amplified
PIWIL2	5.9	38.8	37	18.3	0
EXD1	1.8	36.6	58	3.6	0
DDX4	1.1	20.5	69.3	8.8	0.2
PLD6	0.9	54	42	3.2	0
MOV10L1	0.7	35.7	60.7	2.9	0
ASZ1	0.2	0.9	49.2	49.2	0.5
PIWIL4	0.2	14.2	72.9	12.4	0.2
TDRD1	0.2	21.9	72.9	4.7	0.2
TDRD9	0.2	32.3	60.3	7.2	0
FKBP6	0	1.1	49.7	49	0.2
MAEL	0	9.7	68.8	21	0.5
PIWIL1	0	12.2	68.4	19	0.5
TDRD12	0	6.1	73.4	19.4	1.1
TDRKH	0	9.9	70	19.6	0.5

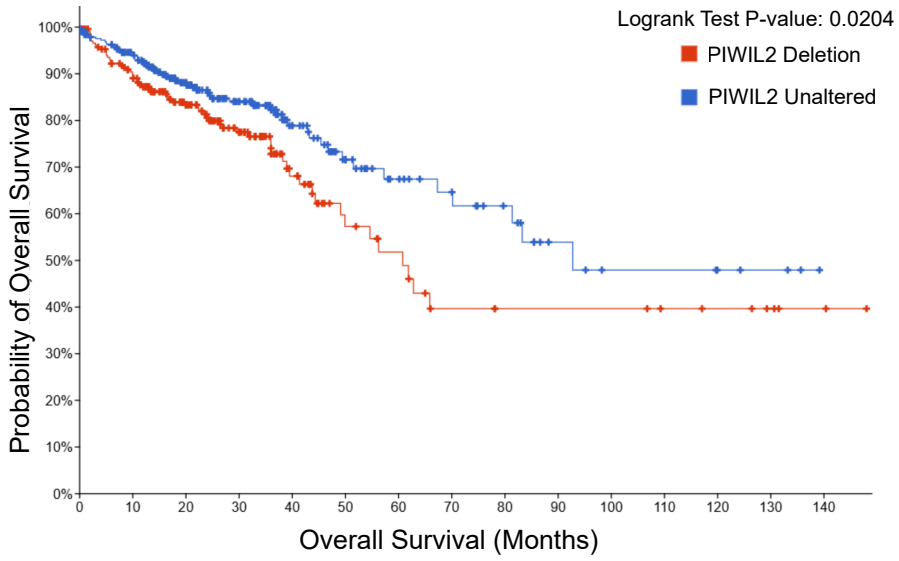

Figure 1

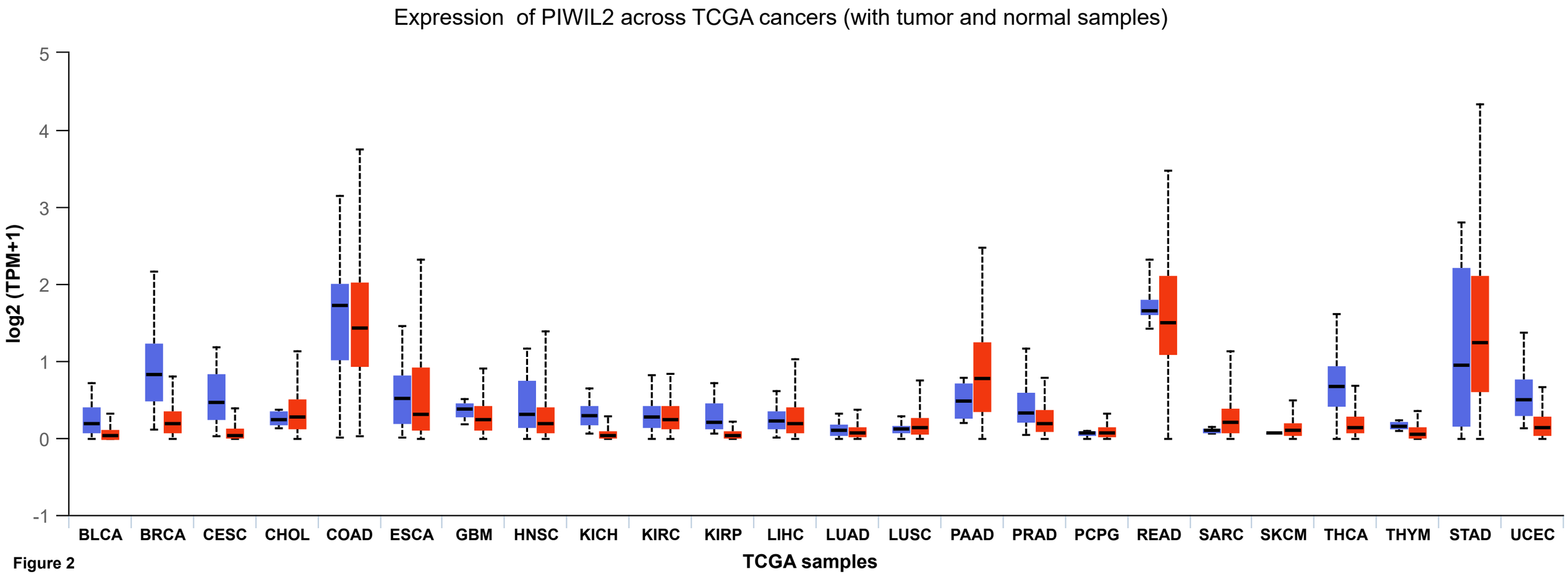
Expression of PIWIL2 across TCGA cancers (with tumor and normal samples)
log2 (TPM+1)
5
4
3
2
1
0
-1
BLCA
BRCA
CESC
CHOL
COAD
ESCA
GBM
HNSC
KICH
KIRC
KIRP
LIHC
LUAD
LUSC
PAAD
PRAD
PCPG
READ
SARC
SKCM
THCA
THYM
STAD
UCEC
TCGA samples

Figure 2

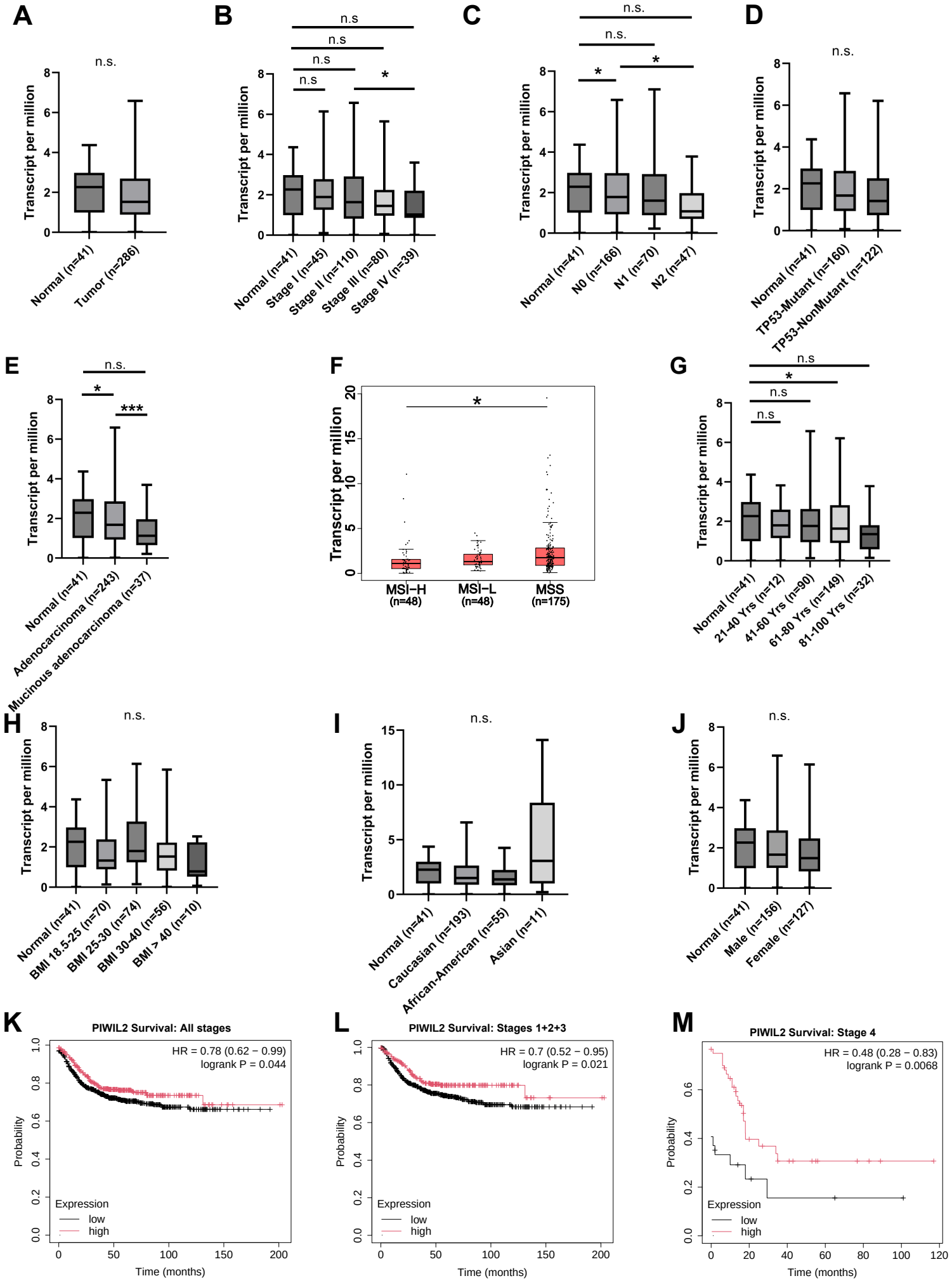
A
n.s.
Transcript per million
Normal (n=41)
Tumor (n=286)
B
n.s
n.s
n.s
n.s
*
Transcript per million
Normal (n=41)
Stage I (n=45)
Stage II (n=110)
Stage III (n=80)
Stage IV (n=39)
C
n.s.
n.s.
*
*
Transcript per million
Normal (n=41)
N0 (n=166)
N1 (n=70)
N2 (n=47)
D
n.s.
Transcript per million
Normal (n=41)
TP53-Mutant (n=160)
TP53-NonMutant (n=122)
E
n.s.
*
***
Transcript per million
Normal (n=41)
Adenocarcinoma (n=243)
Mucinous adenocarcinoma (n=37)
F
*
Transcript per million
MSI-H (n=48)
MSI-L (n=48)
MSS (n=175)
G
n.s
*
n.s
n.s
Transcript per million
Normal (n=41)
21-40 Yrs (n=12)
41-60 Yrs (n=90)
61-80 Yrs (n=149)
81-100 Yrs (n=32)
H
n.s.
Transcript per million
Normal (n=41)
BMI 18.5-25 (n=70)
BMI 25-30 (n=74)
BMI 30-40 (n=56)
BMI > 40 (n=10)
I
n.s.
Transcript per million
Normal (n=41)
Caucasian (n=193)
African-American (n=55)
Asian (n=11)
J
n.s.
Transcript per million
Normal (n=41)
Male (n=156)
Female (n=127)
K
PIWIL2 Survival: All stages
HR = 0.78 (0.62 − 0.99)
logrank P = 0.044
Probability
Expression
low
high
Time (months)
L
PIWIL2 Survival: Stages 1+2+3
HR = 0.7 (0.52 − 0.95)
logrank P = 0.021
Probability
Expression
low
high
Time (months)
M
PIWIL2 Survival: Stage 4
HR = 0.48 (0.28 − 0.83)
logrank P = 0.0068
Probability
Expression
low
high
Time (months)

Figure 3

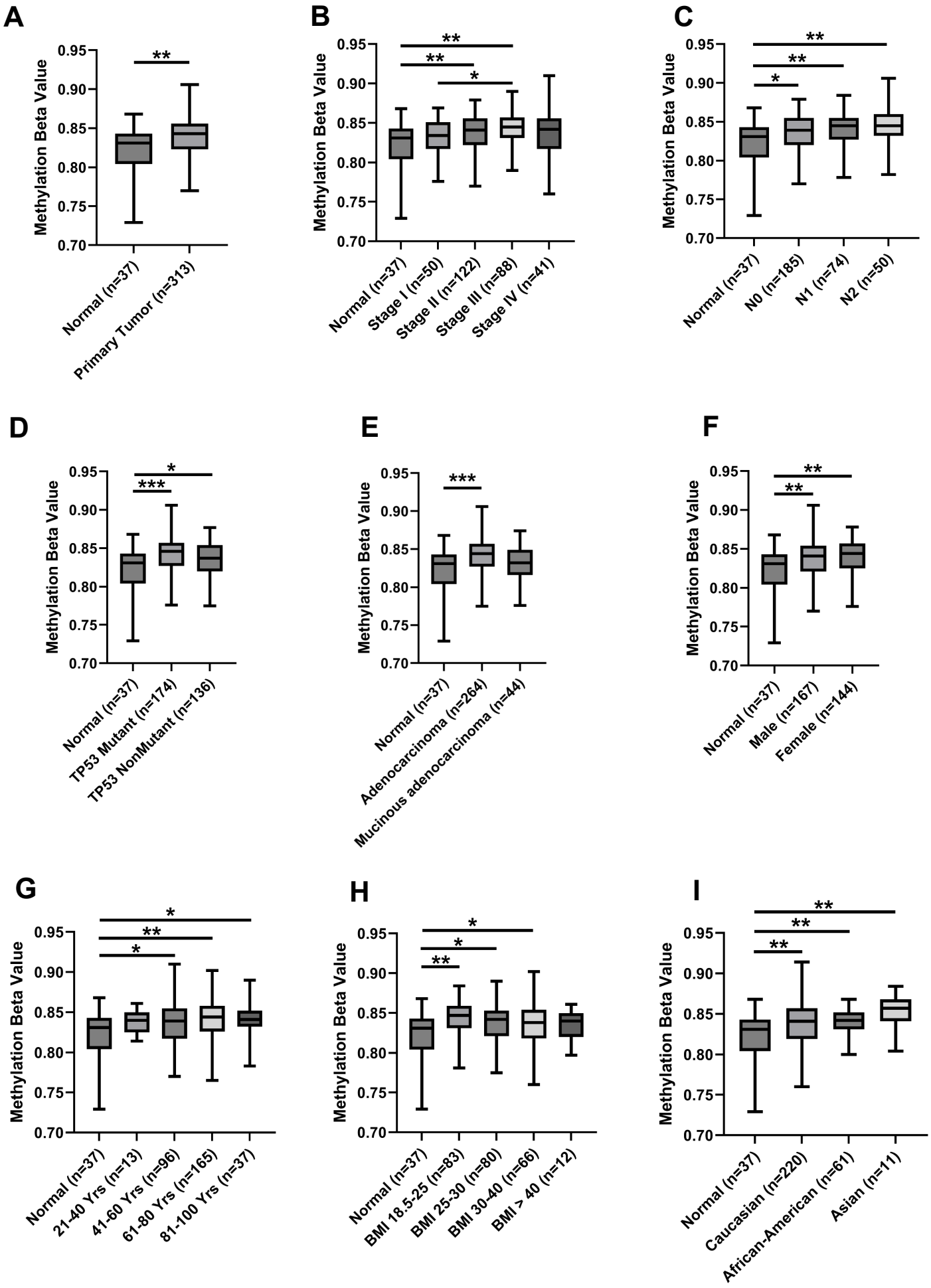
A
Methylation Beta Value
0.95
0.90
0.85
0.80
0.75
0.70
**
Normal (n=37)
Primary Tumor (n=313)
B
**
**
*
Normal (n=37)
Stage I (n=50)
Stage II (n=122)
Stage III (n=88)
Stage IV (n=41)
C
**
**
*
Normal (n=37)
N0 (n=185)
N1 (n=74)
N2 (n=50)
D
*
***
Normal (n=37)
TP53 Mutant (n=174)
TP53 NonMutant (n=136)
E
***
Normal (n=37)
Adenocarcinoma (n=264)
Mucinous adenocarcinoma (n=44)
F
**
**
Normal (n=37)
Male (n=167)
Female (n=144)
G
*
**
*
Normal (n=37)
21-40 Yrs (n=13)
41-60 Yrs (n=96)
61-80 Yrs (n=165)
81-100 Yrs (n=37)
H
*
*
**
Normal (n=37)
BMI 18.5-25 (n=83)
BMI 25-30 (n=80)
BMI 30-40 (n=66)
BMI > 40 (n=12)
I
**
**
**
Normal (n=37)
Caucasian (n=220)
African-American (n=61)
Asian (n=11)

Figure 4

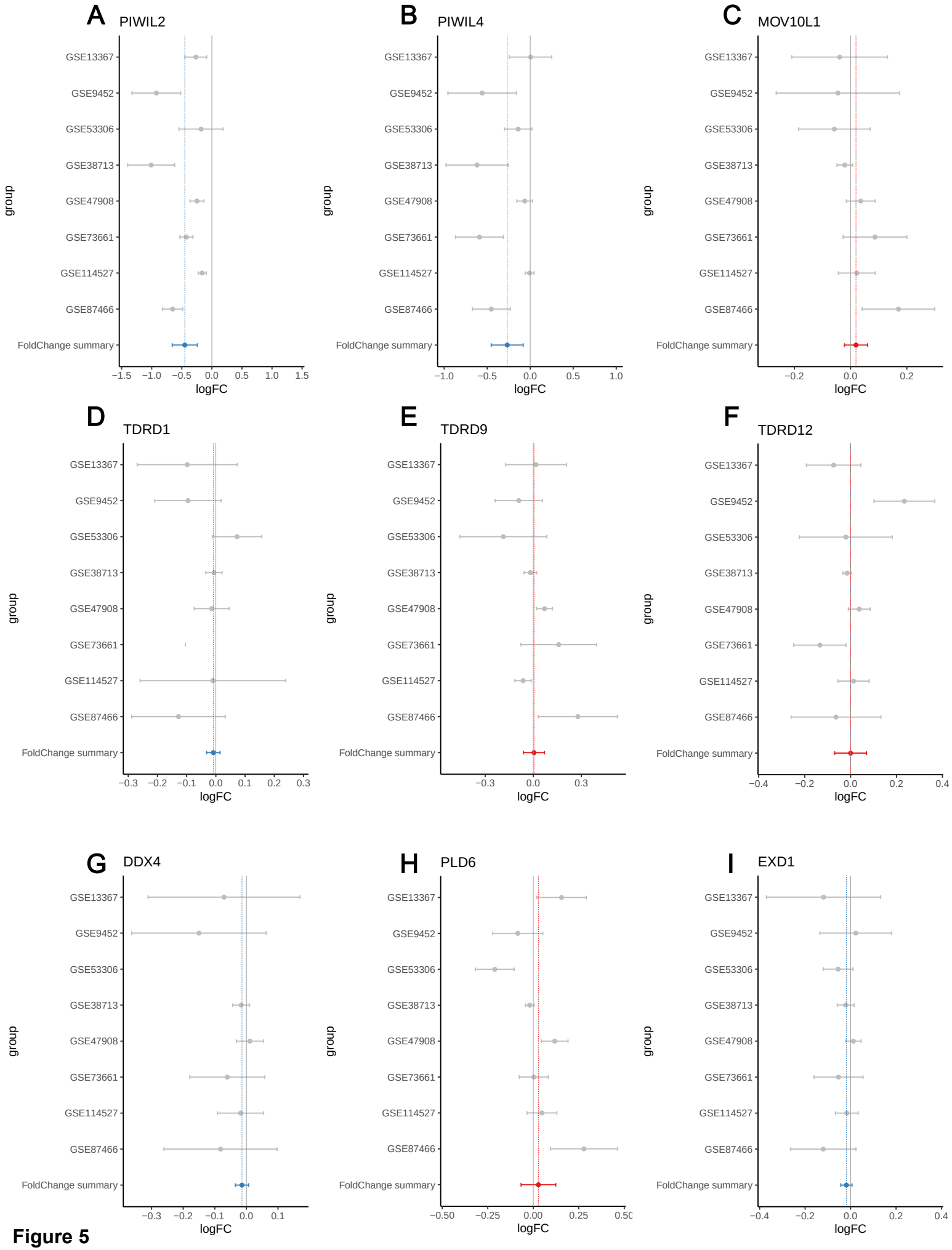
A
PIWIL2
B
PIWIL4
C
MOV10L1
D
TDRD1
E
TDRD9
F
TDRD12
G
DDX4
H
PLD6
I
EXD1
GSE13367
GSE9452
GSE53306
GSE38713
GSE47908
GSE73661
GSE114527
GSE87466
FoldChange summary
group
logFC

Figure 5

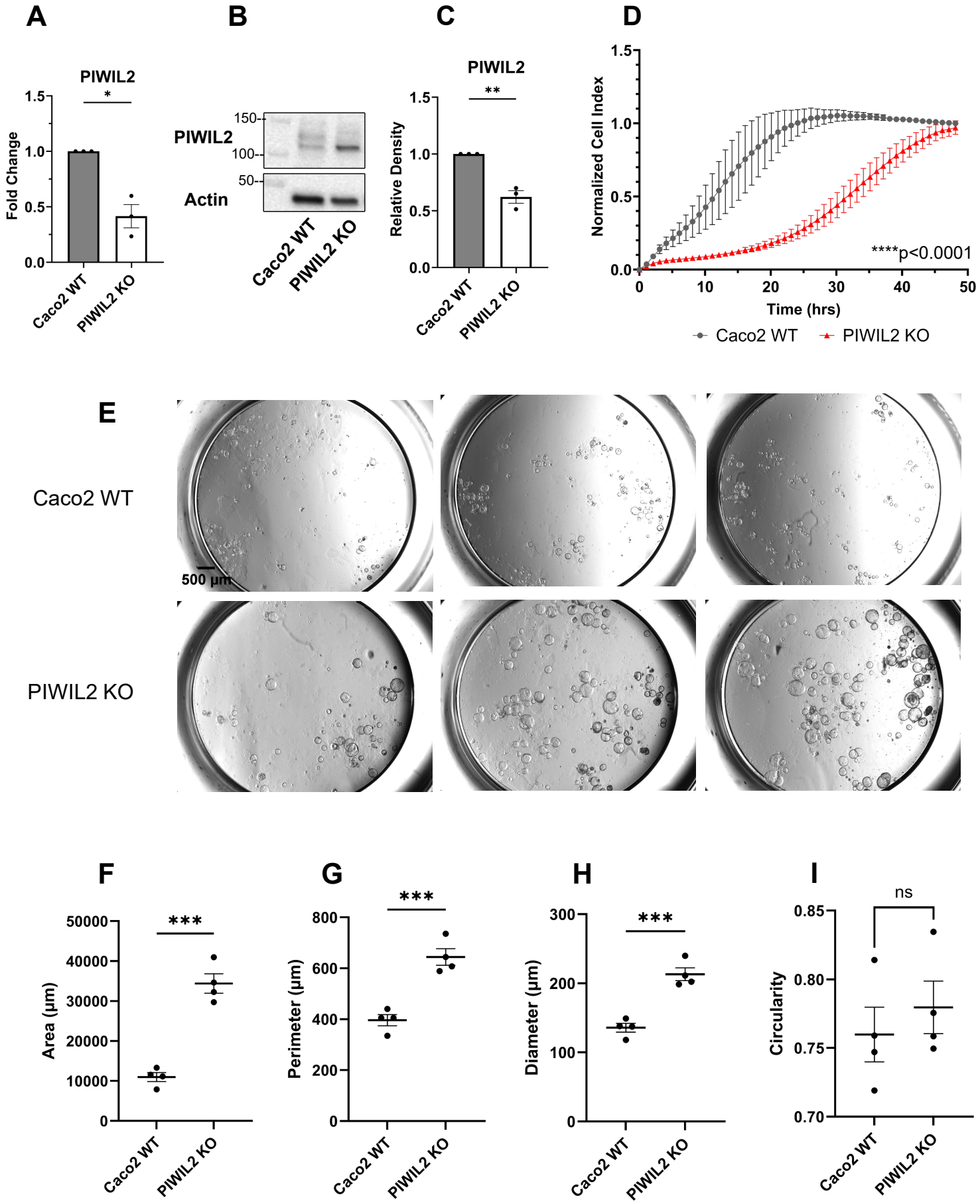
A
PIWIL2
*
Fold Change
1.5
1.0
0.5
0.0
Caco2 WT
PIWIL2 KO
B
150
PIWIL2
100
50
Actin
Caco2 WT
PIWIL2 KO
C
PIWIL2
**
Relative Density
1.5
1.0
0.5
0.0
Caco2 WT
PIWIL2 KO
D
Normalized Cell Index
1.5
1.0
0.5
0.0
****p<0.0001
0
10
20
30
40
50
Time (hrs)
Caco2 WT
PIWIL2 KO
E
Caco2 WT
PIWIL2 KO
500 µm
F
***
Area (µm)
50000
40000
30000
20000
10000
0
Caco2 WT
PIWIL2 KO
G
***
Perimeter (µm)
800
600
400
200
0
Caco2 WT
PIWIL2 KO
H
***
Diameter (µm)
300
200
100
0
Caco2 WT
PIWIL2 KO
I
ns
Circularity
0.85
0.80
0.75
0.70
Caco2 WT
PIWIL2 KO

Figure 6

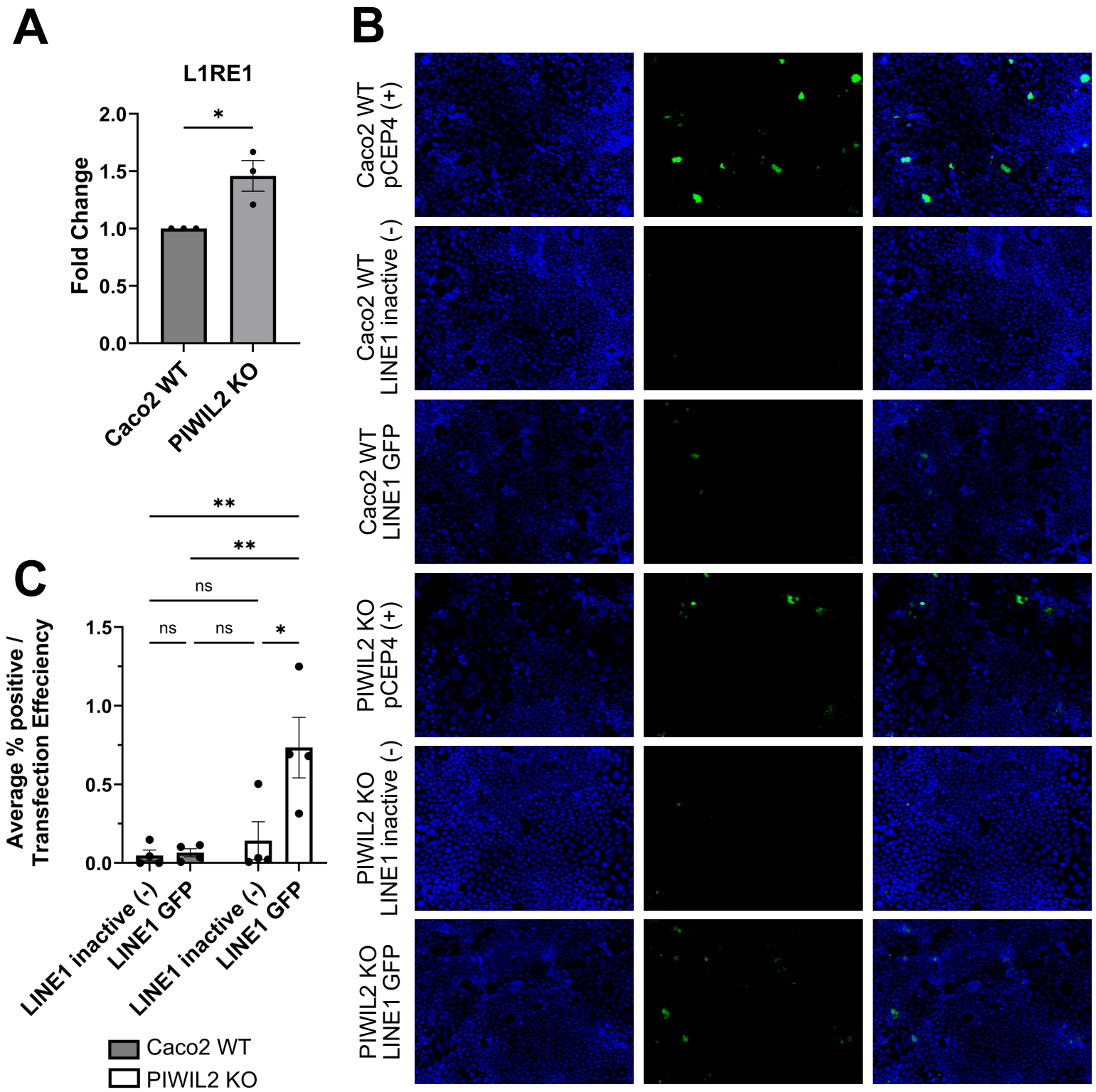
A
L1RE1
Fold Change
2.0
1.5
1.0
0.5
0.0
*
Caco2 WT
PIWIL2 KO
B
Caco2 WT pCEP4 (+)
Caco2 WT LINE1 inactive (-)
Caco2 WT LINE1 GFP
PIWIL2 KO pCEP4 (+)
PIWIL2 KO LINE1 inactive (-)
PIWIL2 KO LINE1 GFP
C
Average % positive / Transfection Effeciency
1.5
1.0
0.5
0.0
**
**
ns
ns
ns
*
LINE1 inactive (-)
LINE1 GFP
LINE1 inactive (-)
LINE1 GFP
Caco2 WT
PIWIL2 KO

Figure 7

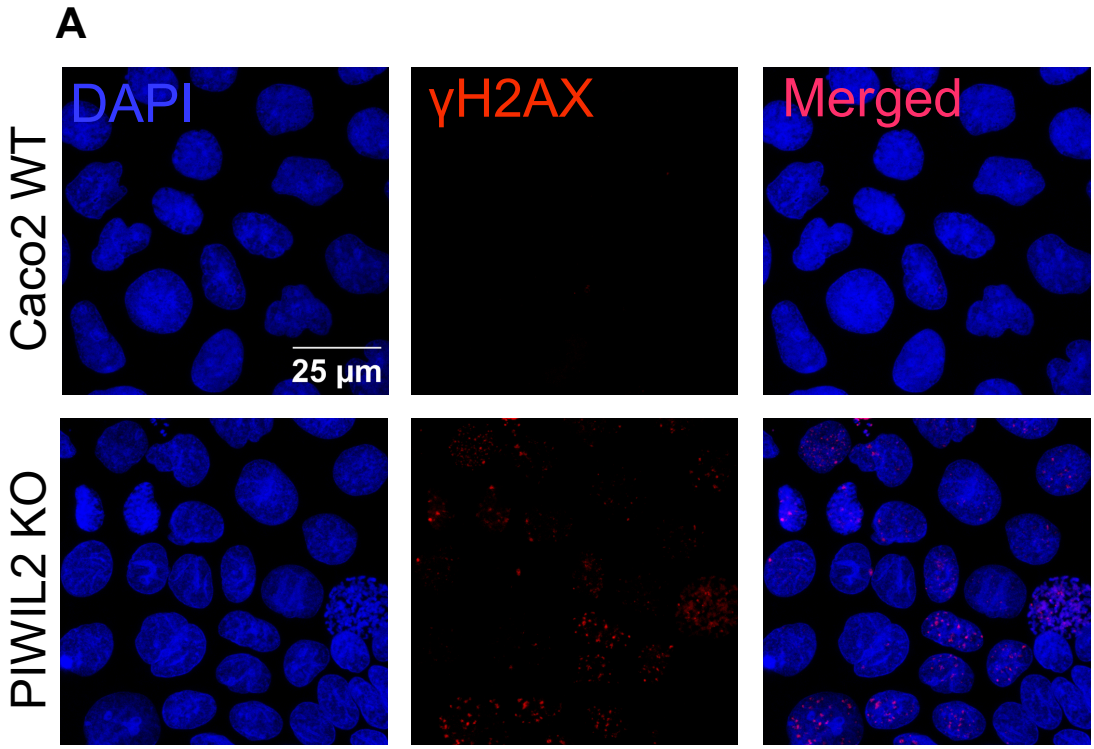
A
DAPI
γH2AX
Merged
Caco2 WT
PIWIL2 KO
25 µm

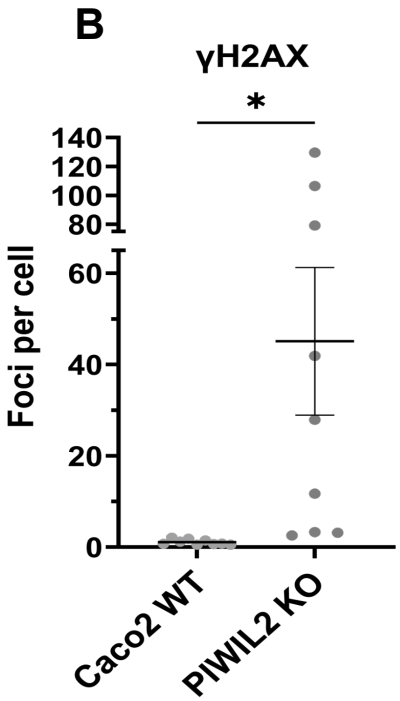
B
γH2AX
*
Foci per cell
140
120
100
80
60
40
20
0
Caco2 WT
PIWIL2 KO

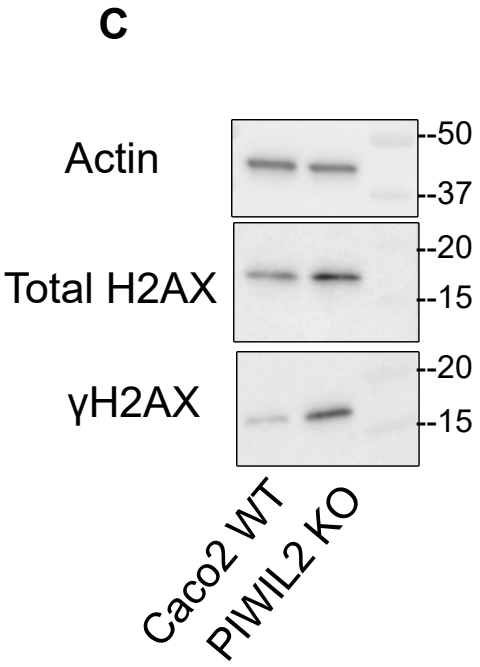
C
Actin
Total H2AX
γH2AX
50
37
20
15
20
15
Caco2 WT
PIWIL2 KO

Figure 8

Table 1. PIWI mRNAs in Caco2 cells		
Symbol	**GeneID**	**avg rpms***
PIWIL1	9271	0.0
PIWIL2	55124	94.7
PIWIL3	440822	19.7
PIWIL4	143689	261.3
*avg reads/million; 3 biological replicates		

Supplemental Table 1

SUPPLEMENTAL MATERIALS

Antibodies

Primary Antibodies

Antibody Name	Company	Catalogue Number	Animal	WB dilution	IF dilution
PIWIL2	Sigma Aldrich	SAB3500749	Rb	1 to 1000	-
β-actin (Actin)	Cell Signaling	4967L	Rb	1 to 2000	-
H2AX total	Santa Cruz	sc517336	Ms	1 to 1000	-
γH2AX	Cell Signaling	20 E3 (9718T)	Rb	1 to 1000	1 to 400 (MeOH Fixed)

Secondary Antibodies

Antibody Name	Company	Catalogue Number	Animal	WB dilution	IF dilution
HRP-anti-rabbit	Jackson ImmunoResearch	711-035-152	Rb	1 to 2000	-
HRP-anti-mouse	Jackson ImmunoResearch	715-035-150	Ms	1 to 2000	-
Alexafluor 647 anti-mouse	Invitrogen	A21236	Ms	-	1 to 500 (MeOH Fixed)

qPCR Probes

Probe name	Company	Assay ID
18S	Thermo Fisher	Hs99999901_s1
PIWIL2	Thermo Fisher	Hs01032719_m1
L1RE1(APFVNJ2)	Thermo Fisher	custom sequence